



HAL
open science

Giant Star-shaped meso -substituted Fluorescent Porphyrins with Fluorenyl-containing Arms Designed for Two-photon Oxygen Photosensitization

Limiao Shi, Zhipeng Sun, Nicolas Richy, Mireille Blanchard-Desce, Olivier Mongin, Frédéric Paul, Christine Odile Paul-Roth

► **To cite this version:**

Limiao Shi, Zhipeng Sun, Nicolas Richy, Mireille Blanchard-Desce, Olivier Mongin, et al.. Giant Star-shaped meso -substituted Fluorescent Porphyrins with Fluorenyl-containing Arms Designed for Two-photon Oxygen Photosensitization. *Chemistry - A European Journal*, 2024, 30 (13), 10.1002/chem.202303243 . hal-04455880

HAL Id: hal-04455880

<https://hal.science/hal-04455880>

Submitted on 13 Feb 2024

HAL is a multi-disciplinary open access archive for the deposit and dissemination of scientific research documents, whether they are published or not. The documents may come from teaching and research institutions in France or abroad, or from public or private research centers.

L'archive ouverte pluridisciplinaire **HAL**, est destinée au dépôt et à la diffusion de documents scientifiques de niveau recherche, publiés ou non, émanant des établissements d'enseignement et de recherche français ou étrangers, des laboratoires publics ou privés.

Giant Star-shaped *meso*-substituted Fluorescent Porphyrins with Fluorenyl-containing Arms Designed for Two-photon Oxygen Photosensitization

Limiao Shi,^a Zhipeng Sun,^a Nicolas Richey,^a Mireille Blanchard-Desce,^b Olivier Mongin,^a Frédéric Paul,^a Christine O. Paul-Roth,^{a,*}

Dedicated to Professor Ken RAYMOND for his fascinating work in Bioinorganic Chemistry, as well as for his very remarkable birthday (with a little delay)

^a *Dr. L. Shi, Dr. Z. Sun, N. Richey, Dr. O. Mongin, Dr. F. Paul, Dr. C. O. Paul-Roth*

Univ Rennes, INSA Rennes, CNRS, ISCR (Institut des Sciences Chimiques de Rennes) – UMR 6226, F-35000 Rennes, France.

^b *Dr. M. Blanchard-Desce*

Univ. Bordeaux, Institut des Sciences Moléculaires (CNRS UMR 5255), 33405 Talence, France.

*Corresponding author: christine.paul@univ-rennes1.fr or christine.paul@insa-rennes.fr

tel : (+33) (0) 2 23 23 63 72

Abstract: In the continuation of previous studies on carbon-rich *meso*-tetraarylporphyrins featuring 2,7-fluorene units at their periphery, the effect of changing the peripheral dendritic arms for linear arms on their oxygen-photosensitizing ability, their fluorescence and their two-photon absorption (2PA) properties is now analyzed. Thus, starburst porphyrins possessing up to twenty conjugated fluorenyl units were isolated and studied. More precisely, a series of five new free-base porphyrins featuring fully conjugated arms incorporating an increasing number of fluorenyl groups connected *via* 1,2-alkenyl spacers were synthesized, along with their Zn(II) complexes. Upon excitation in the arm-centred π - π^* absorption band, an efficient energy transfer takes place from the peripheral fluorenyl units to the central porphyrin core, leading to intense red-light emission and oxygen photosensitization by the latter. More interestingly, while the linear optical properties of these porphyrins were only slightly improved compared to those of their dendrimer analogues for photodynamic therapy (PDT) or fluorescence imaging, their 2PA cross-sections were much more significantly boosted, evidencing the key role played by different structures on nonlinear optical properties. Finally, by comparison with other porphyrin-based two-photon photosensitizers reported in the literature, we show that these new “semi-disconnected” starburst systems exhibit a remarkable trade-off between intrinsic 2PA, fluorescence and oxygen photosensitization.

Keywords

Porphyrinoids • Fluorene • Two-photon absorption • Oxygen sensitization • Fluorescence • Energy transfer

Introduction

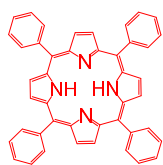
Meso-tetraarylporphyrins are particularly interesting systems because the peripheral arms on the macrocyclic core can modulate the physical properties of the tetrapyrrolic core at will. For example, when the arms are substituted in a dendrimeric way around the core,^[1] the resulting compounds form a wonderful class of dendrimers presenting peripheral branches with a tree-like structure (dendrons). In selected cases,^[2] these dendrons work as efficient “light-harvesting antennas” recalling those collecting natural light in various photosystems. Thus, after excitation with UV or visible light, they quantitatively transfer their energy to the central porphyrin core where it can be advantageously used in various physicochemical processes.^[3a, 3b, 3c-e] For oligoarylether scaffolds, Fréchet demonstrated that such an “*antenna effect*” was more efficient in highly branched dendrimeric architectures than in linear star-shaped architectures.^[3b]

In such systems, besides the topology (branching) of these peripheral dendrons, their chemical structure can also be of importance for enhancing other properties such as two-photon absorption (2PA).^[4] Thus, we have previously shown that when going from non-conjugated dendrons^[5a-c, 5d, 5e] to more rigid carbon-rich analogues such as the tetraphenylporphyrin (TPP)-cored family of compounds **1a-c** (Scheme 1),^[6] the quantum yields for two-photon excited fluorescence (2PEF) and two-photon oxygen photosensitization (2POS) were significantly improved compared to similar systems featuring less π -interacting aromatic units.^[5e, 6b] In line with investigations made on other families of two-photon absorbers,^[7] we then found that related architectures such as **2b**, in which double bonds replaced triple bonds in previous **1b**, were even better suited to such tasks.^[8] Further improvements of these properties relative to **1a-**

c were then obtained by replacing the central **TPP** core by a *meso*-tetrafluorenylporphyrin (**TFP**) core in which the *meso*-phenyl groups of **TPP** were replaced by 2-fluorenyl ones (**3a-c**; Scheme 1),^[9] the various *n*-butyl chains on the fluorenyl groups helping for solubilizing these “extended” analogues of **1a-c** in common solvents.^[6, 9] The latter systems were particularly promising for developing new photosensitizers (PS) for one-^[10] and two-photon photodynamic therapy (1P-PDT and 2P-PDT, resp.),^[11] but also for related theranostic uses.^[12] This could be done after water-solubilizing these systems, (i) either by proper functionalization of the model compounds or (ii) by encapsulation into biocompatible nanoparticles.^[13]

Previous Work

References

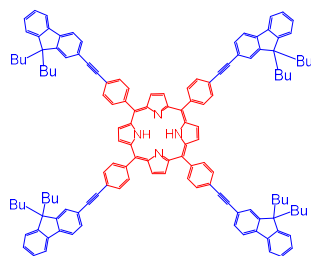


TPP

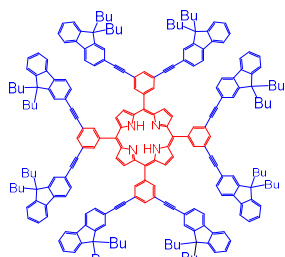


TFP

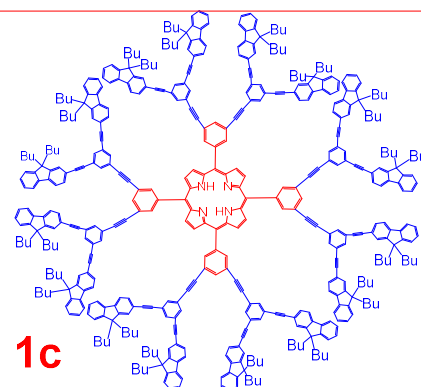
TPP-based Dendrimers



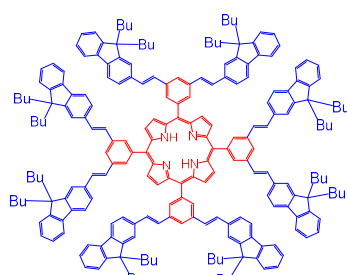
1a



1b

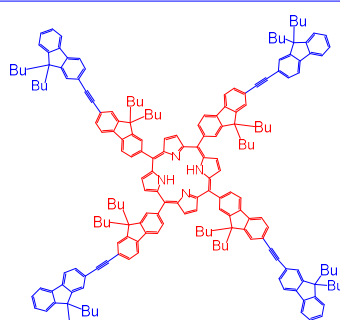


1c

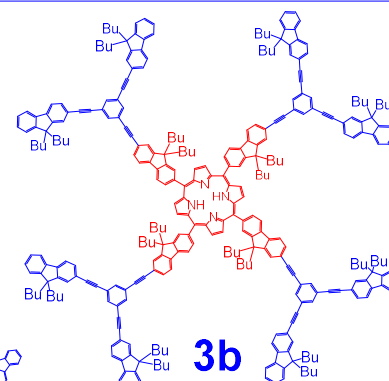


2b

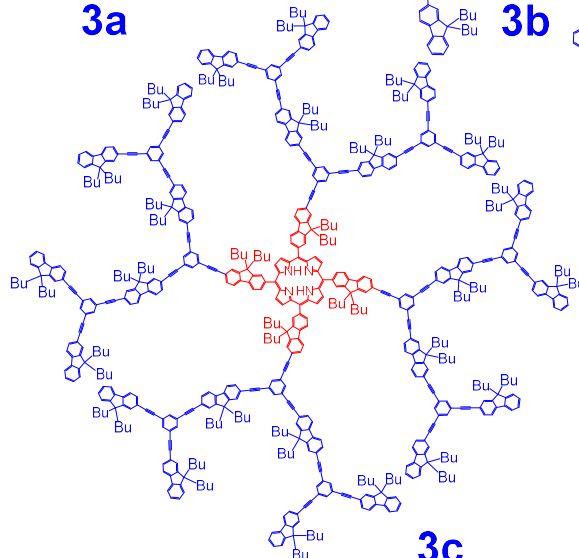
TPP-based Dendrimer



3a



3b

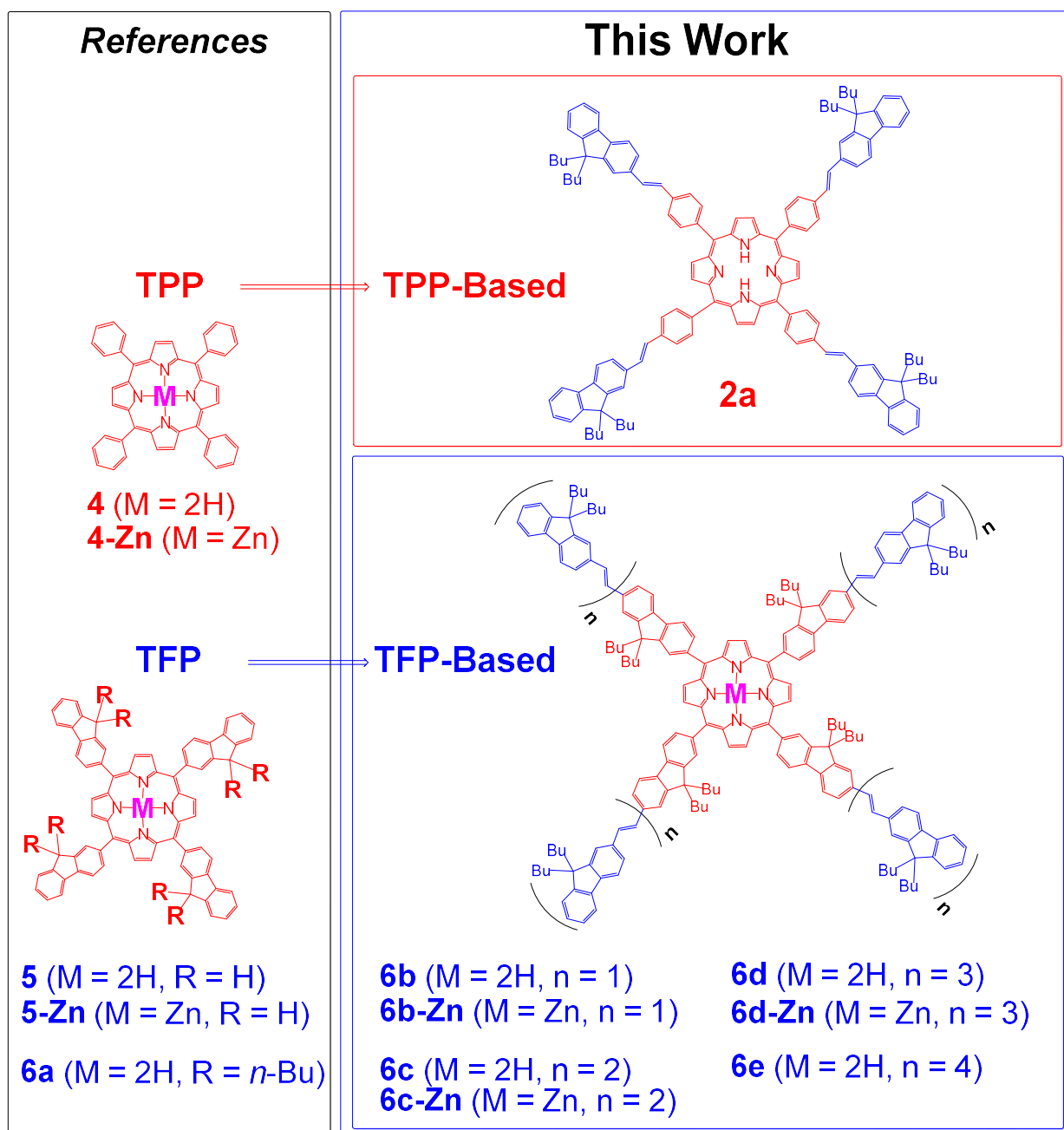


3c

TFP-based Dendrimers

Scheme 1. Molecular structures of references **TPP** and **TFP**, along with various generations of **TPP-based (1a-c, 2b)** and **TFP-based (3a-c)** dendrimers featuring conjugated fluorenyl units in their peripheral arms.

Interestingly, based on relevant figures of merit,^[5e] it appeared from these studies that star-shaped architectures were the most suited for 2PEF and 2POS.^[13a] Actually, to the best of our knowledge, apart from the seminal work of Bo and co-workers,^[3c, 3d] very few subsequent studies have been conducted on the photosensitizing properties of well-defined star-shaped porphyrins incorporating 2,7-fluorenyl groups at their periphery^[14] and virtually none on their 2PA properties.^[15] Thus, only few structure-property relationship emerged for identifying key structural features allowing to optimize 2PEF and 2P-PDT. Nevertheless, these researchers were the first to point out the positive role of the **TFP** core (**5**, Scheme 2) for enhancing the fluorescence quantum yield of such starburst systems,^[3d] a statement that some of us confirmed independently, by stating that the quantum yield of **TFP** (24%) was twice that of **TPP** (11%).^[5a-c] Later on, with **6a** and **3a-c**^[9] we also showed that replacement of *meso*-1,4-phenylene units by 2,7-fluorenyl ones significantly increases the 2PA cross-sections of the corresponding systems without affecting the other photophysical properties of interest.



Scheme 2. TPP and TFP used as reference compounds and targeted corresponding model compounds.

Given that 1,2-alkene spacers in **2b** were shown to promote 2PA better than 1,2-alkyne ones in **1b**^[8] and given that star-shaped architectures such as **1a** or **3a** present better figures of merit for 2PEF than higher generation dendrimers,^[6b,9] it was now sensible to explore the linear and nonlinear photophysical properties of star-shaped molecules featuring poly(1,2-alkenyl-

2,7-fluorenyl) arms of increasing length such **6b-e** (Scheme 2). During this work, the **TPP**-analogue (**2a**) of **6b** was also targeted for comparison purposes. Furthermore, given that metallation of the porphyrin by a transition metal center could potentially increase the 2P-PDT performances of these photosensitizers, either by boosting the 2PA cross-sections, due to the presence of a polarisable transition metal atom in the tetrapyrrolic ring,^[16] or by favoring oxygen photosensitization, due to faster intersystem crossing (heavy atom effect),^[17] we have decided to also investigate the photophysical properties of some Zn(II) complexes of **6b-e** (**6b/d-Zn**).

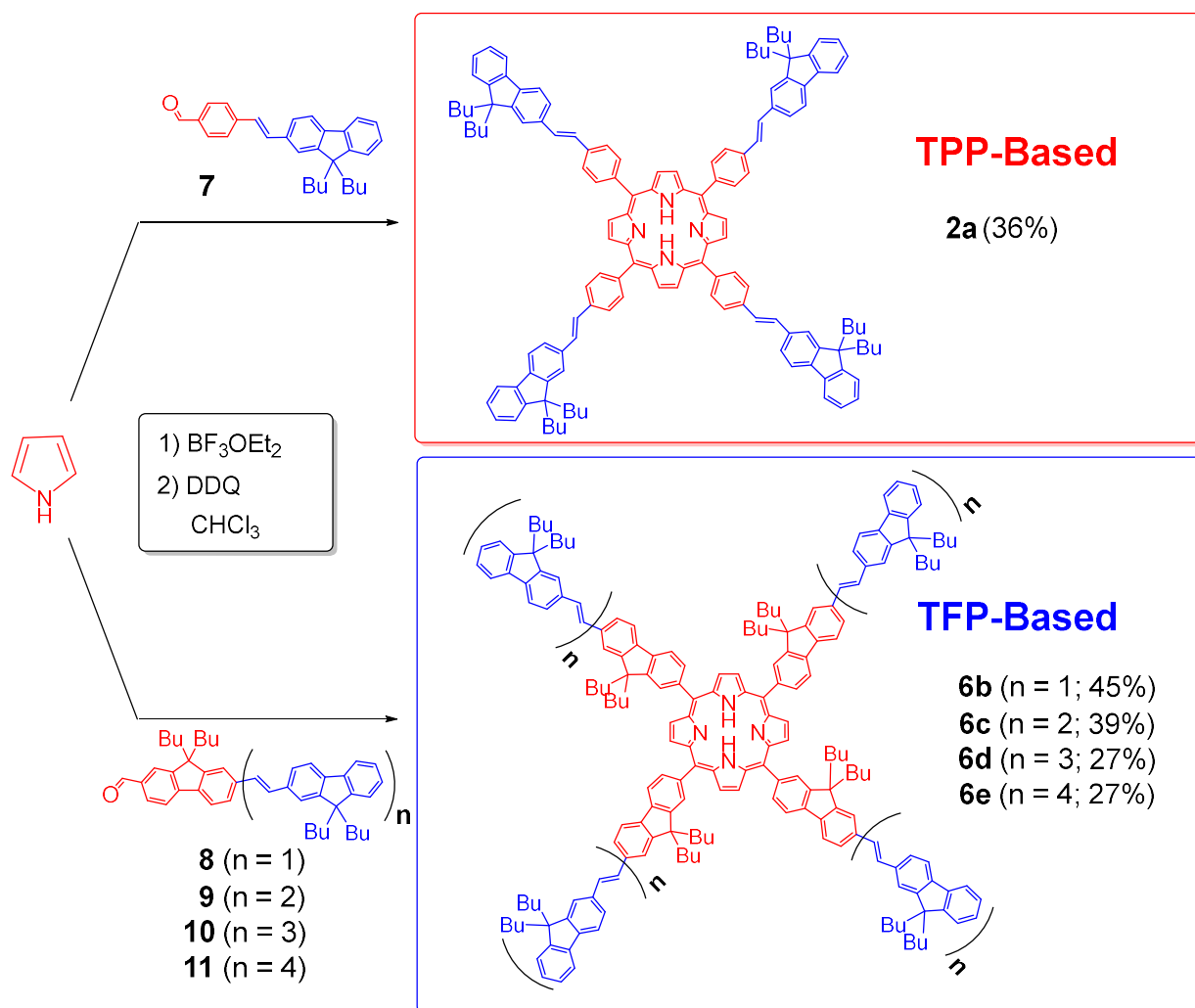
Results and Discussion

The synthesis of these new star-shaped free-base porphyrins was carried out from pyrrole and the corresponding aldehydes, as detailed below. The synthesis and characterization of their Zn(II) complexes is then next briefly described, before discussing the optical properties of interest of these compounds.

Synthesis and characterization of the targeted porphyrins

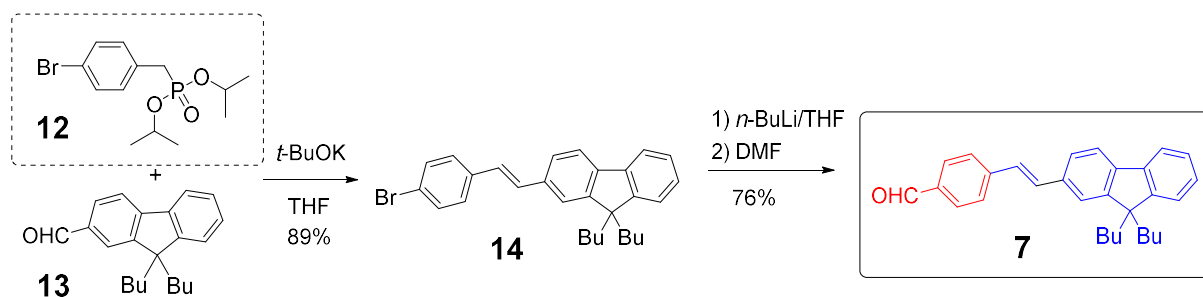
Synthesis of the free-base porphyrins 2a and 6b-e. Porphyrins **2a** and **6b-e** were all obtained *via* a classical condensation/oxidation reaction between the aldehydes (**7**, **8**, **9**, **10** and **11**) and pyrrole, under mild Lindsey conditions (Scheme 3).^[18] As expected, the macrocyclization yields decrease as the *meso*-arms lengthen (from 45% to 27%). Given that the aldehyde precursors were all new, we will also describe below the synthesis of the benzaldehyde **7**, followed by the

synthesis of the parent 2-fluorenaldehydes **8**, **9**, **10** and **11** obtained in an iterative approach from a common set of reactions. Starting from their common fluorenaldehyde precursor (**13**), once the required phosphonate (**12** or **15**; Schemes 4-5) were available, the porphyrins **2a** and **6b-e** were obtained in 36%, 45%, 39%, 27% and 27% total yield, respectively. All these star-shaped compounds were characterized by NMR, HRMS and elemental analysis after chromatographic purification and recrystallization. It was shown by ¹H NMR that the *E*-configuration is maintained in all compounds, except for **2a**, which possibly isomerizes in solution. Its stereochemical stability was monitored in solution by ¹H NMR studies in CDCl₃ (ESI, Figure S20). The appearance of new signals (AB systems) for *meso*-phenyl groups (*J* = 7.8 Hz) around 8.5 ppm was stated. Based on similar studies made on the aldehyde precursors **7-11** (ESI, Figures S18 and S19), we tentatively propose that an *E-Z* configurational change takes place in some of the peripheral arms of **2a**. Such a change was however not observed for **6b-d**.



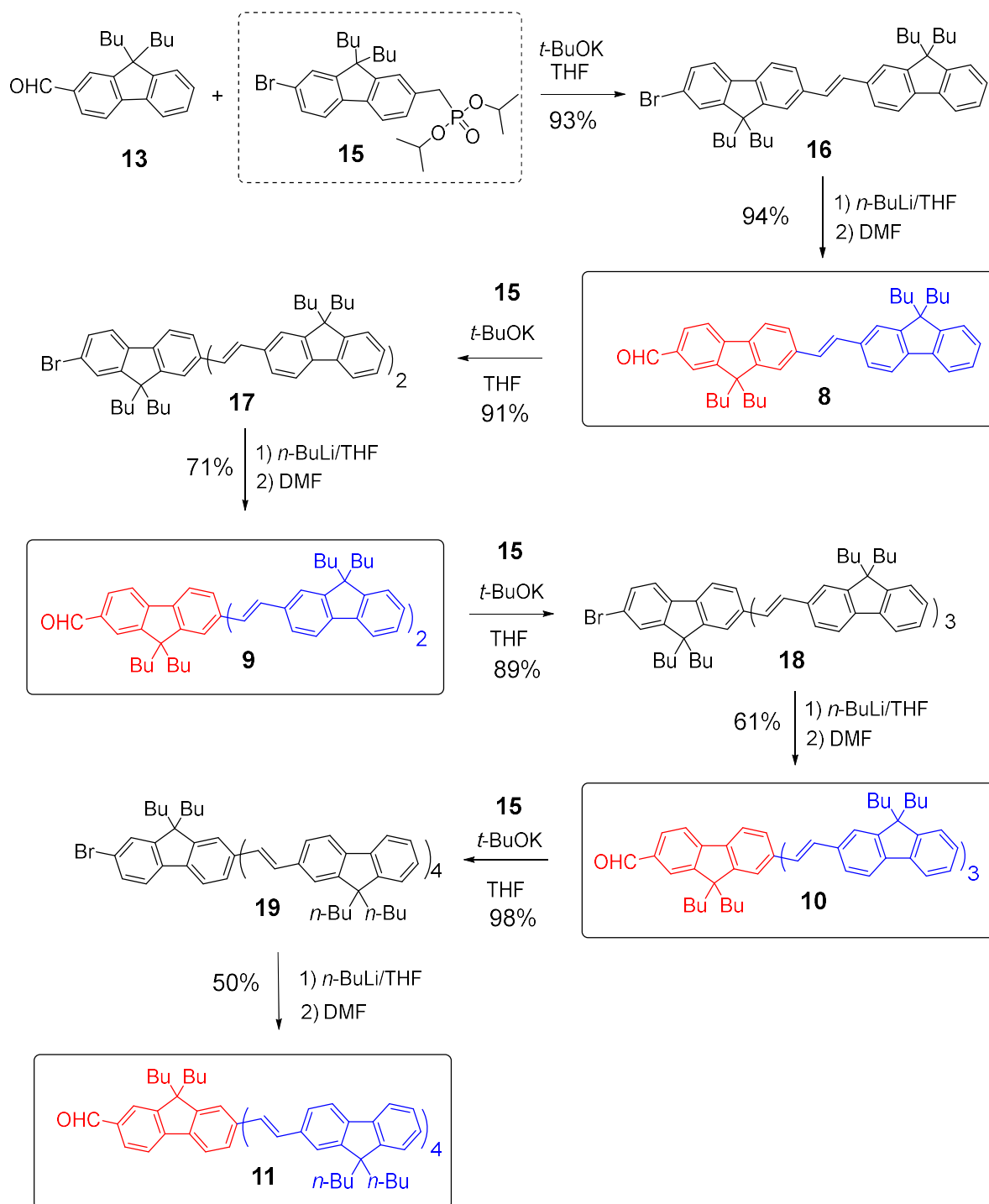
Scheme 3. Synthesis of the star-shaped porphyrins **TPP-based 2a** and **TFP-based 6b-e**.

Synthesis of the target aldehydes 7, 8, 9, 10 and 11. The benzaldehyde **7** was synthesized in two steps from the phosphonate **12** and 2-fluorenaldehyde (**13**) *via* a Horner-Wadsworth-Emmons (HWE) reaction under basic conditions^[19] to give intermediate **14**, isolated as the *E*-stereoisomer, followed by lithiation and subsequent formylation using DMF in a one-pot reaction. The desired benzaldehyde **7** was isolated in an overall yield of 68% after purification (Scheme 4).



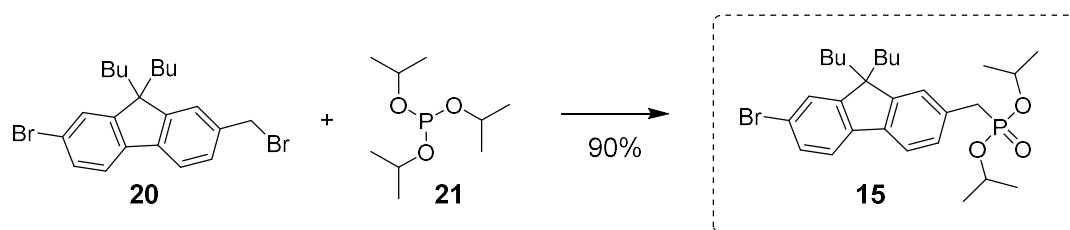
Scheme 4. Synthesis of benzaldehyde **7** from 2-fluorenylaldehyde **13**.

The four 2-fluorenyl aldehydes **8-11** were obtained similarly from 2-fluorenylaldehyde **13** and 2-bromofluorenyl phosphonate **15**, using sequences of alternating HWE reactions and lithiation/formylation reactions in an iterative approach (Scheme 5). These derivatives were isolated as *E*-stereoisomers, as ascertained by ^1H NMR (by diagnostic $^3J_{\text{HH}}$ coupling constants of alkene protons of 16 Hz), in good total yields, after purification by silica column chromatography (87% for **8**; 56% for **9**; 31% for **10** and 15% for **11**).



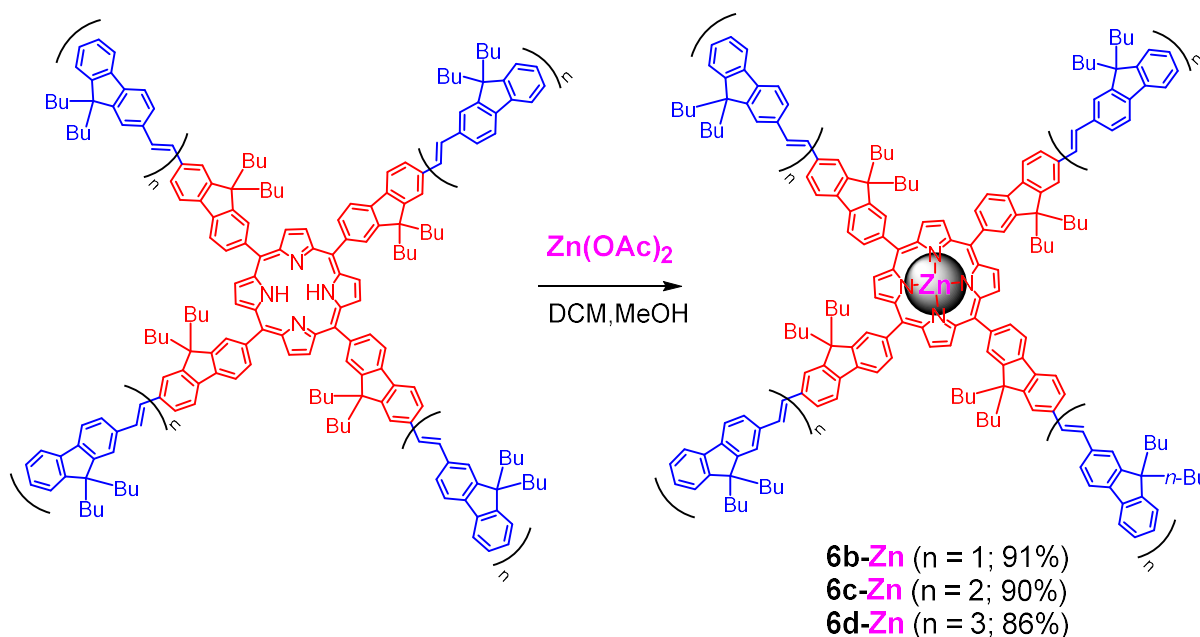
Scheme 5. Synthesis of four double bonded fluorenaldehydes **8-11**.

Likewise to **12**,^[20] the starting phosphonate reactant **15** was obtained following an Arbuzov reaction (Scheme 6).^[21] It was isolated in 90% yield from 2-bromo-7-(4-bromomethyl)fluorene (**20**) and commercial triisopropylphosphite (**21**).



Scheme 6. Formation of the intermediate 2-fluorenyl phosphonate **15**.

Synthesis of the Zn(II) porphyrins 6b-d-Zn. Given that **2a** turned out to be configurationally labile in solution (ESI, Figure S20), only the most readily available free bases **6b-d** were subjected to complexation by Zn(II). The corresponding zinc complexes **6b-Zn**, **6c-Zn** and **6d-Zn** were obtained in good yields (86-91%) after metalation using zinc acetate, in a mixture of dichloromethane and methanol (Scheme 7). These Zn(II) complexes were purified by recrystallization and characterized as described before. Their stereoisomeric purity (*E*) after complexation was confirmed by ^1H NMR (ESI).



Scheme 7. Synthesis of three zinc porphyrin complexes **6b-Zn**, **6c-Zn** and **6d-Zn**.

Optical properties

One- and two-photon absorption (1PA and 2PA) and emission properties, as well as oxygen photosensitization properties were next determined for these porphyrin families in various solvents (CH₂Cl₂, toluene or THF) using known *meso*-tetraaryl porphyrins like **TPP** (**4**), **TFP** (**5**) and the more soluble **TFP** with butyl chains (**6a**) for benchmarking the properties of the unsubstituted dendrimer core (Scheme 2). While **4** was always our usual reference for previous porphyrin-based dendrimers such as **1a-c** or **2b**,^[6b, 8] comparison of **6b-e** with **5** or **6a** allows to better evidence the effect of the extra fluorenyl groups at the periphery (*i.e.* in the dendrons) on the optical properties.^[9] For more clarity, we will discuss these results in two separate parts: (i) free-base porphyrins and (ii) zinc complexes.

One photon absorption and emission spectra. The one-photon absorption spectra of all these new-star shaped porphyrins were recorded between 250 and 800 nm and their emission spectra between 400 (or 550) and 800 nm (Figures 1-2 and Table 1).

Free-base porphyrins. For compounds **2a**, **6b-e** in CH₂Cl₂, feature the characteristic absorption bands of porphyrins which are: (a) an intense Soret-band around 420-440 nm and (b) four Q-bands from 520-660 plus an additional absorption band around 340-420 nm, which corresponds to the lowest π - π^* transition of the four conjugated arms (Figure 1a) as demonstrated by the comparison between the absorption spectra of porphyrins **6b-e** and their corresponding aldehyde precursors (**8-11**), respectively (ESI, Figure S38). This intense fluorenyl-based absorption, is absent for **TPP** (**4**) but also for **TFP** (**6a**) references, which suggests that the unconjugated *meso*-fluorenyl groups of **6a** absorb below 280 nm, whilst the extended and

conjugated fluorenyl arms of free bases from **2a** and **6b-e**, are strongly red shifted (341-419 nm) and much more intense. Thus, after normalizing the spectra to the intensity of the Soret-band, this arm-based absorption increases regularly with increasing length upon going from **6a** to **6e** (even when including **2a** in the series), roughly scaling with the number of fluorenyl groups in each peripheral arm. The strong bathochromic shift observed when progressing from **6a** to **6e** reflects that observed in the starting aldehydes **8-11** and reveals efficient conjugation through the *alkene bonds*. Actually, it appears very similar to that observed for **1a** (323 nm) and **3a** (340 nm), the alkyne analogues of **2a** and **6b**, respectively (Figure 1b). In this respect, the shift of the Soret band (419-446 nm), which follows the same trend between **6a** and **6e**, likely reflects the conjugation of the central porphyrin core with the peripheral dendrons in these compounds.

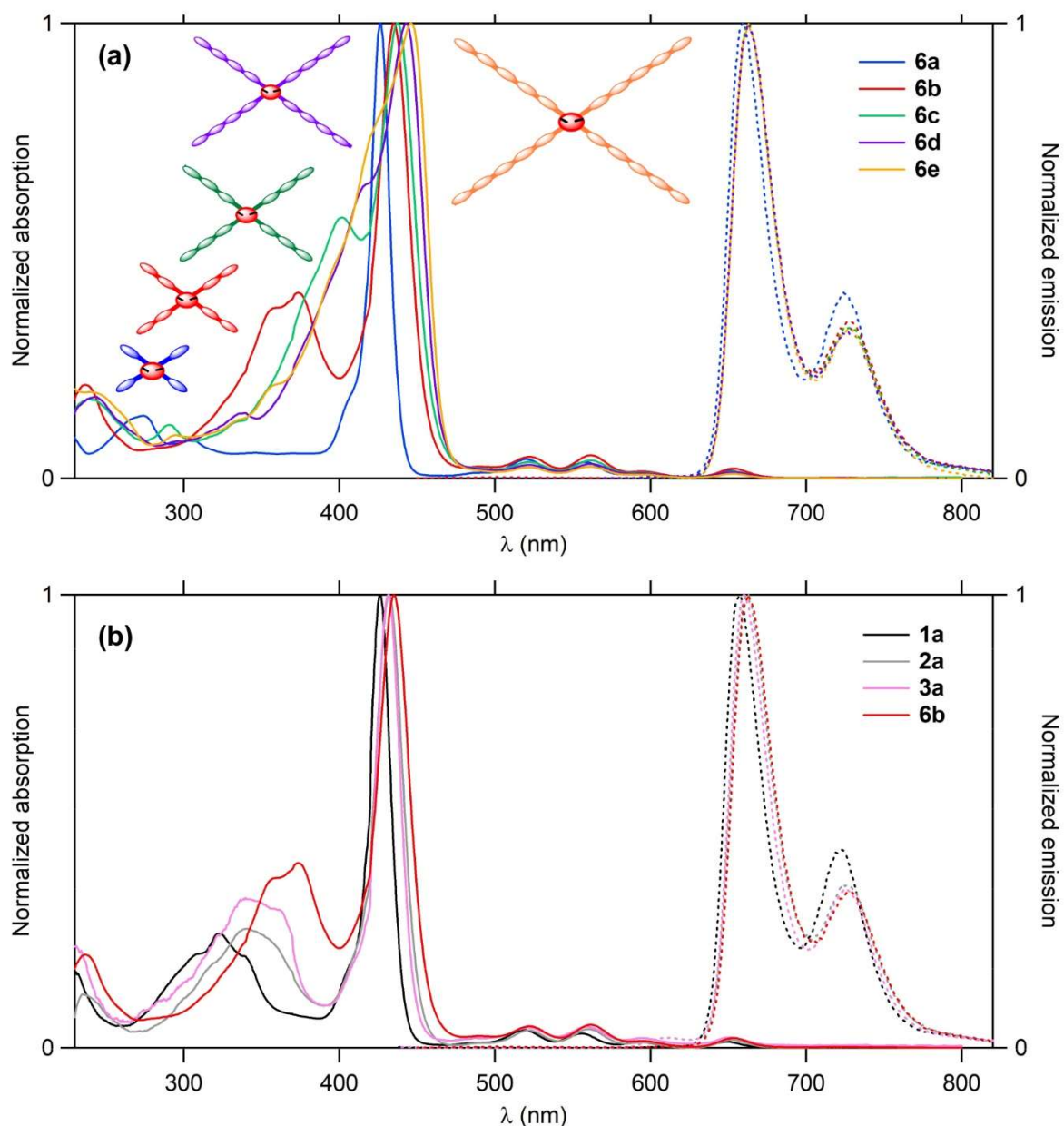


Figure 1. (a) Normalized UV-visible absorption and emission spectra of free-base porphyrins **6a-e** in air-equilibrated CH_2Cl_2 solutions, upon excitation at the maximum of the Soret band. (b) Normalized UV-visible absorption and emission spectra of free-base porphyrins **1-3a** and **6b** in CH_2Cl_2 .

The emission spectra of these free-base porphyrins in CH_2Cl_2 after excitation in the Soret-band (Figure 1) and also after excitation in the arm-centered π - π^* band (Figure 2) reveal the characteristic porphyrin emission peaks Q(0,0) and Q(0,1). After normalizing the emission intensities of these compounds to their Q(0,0) peaks, all five derivatives exhibit very similar

emission spectra with a constant intensity ratio between Q(0,0) and Q(0,1), suggesting a similar electronic influence on the porphyrin core along the series.

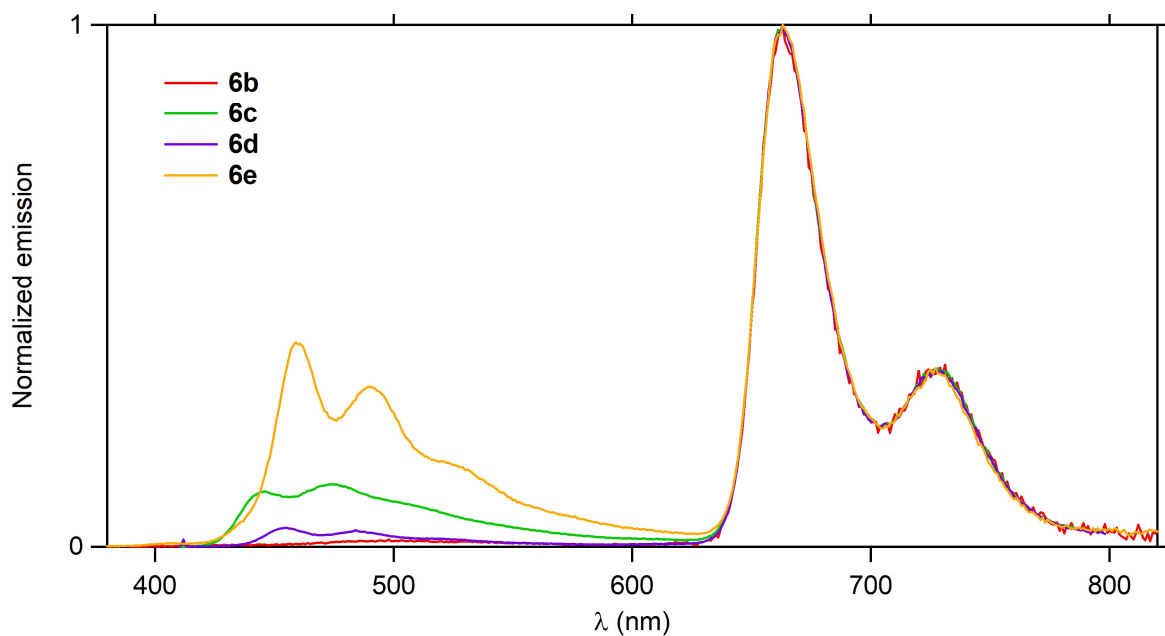


Figure 2. Normalized emission spectra of the free-base porphyrins **6b-e**, in CH₂Cl₂ upon excitation at 350 nm.

The comparison of the data gathered for **2a**, **6b-e** with **TPP** (**4**) or **TFP** functionalized with *n*-butyl chains (**6a**), used as references (Scheme 2), reveals similar fluorescence quantum yields for the **TFP**-cored derivatives (**6b**) compared to their phenyl-cored analogues (**2a**) (Table 1). Thus, the emission quantum yields for the entire series **6b-e** (20-22 %) are slightly higher than that of the free-base **6a** (18%) and much more than those of **TPP**-cored homologues.^[6b]

Table 1. Photophysical properties of the new porphyrins **2a** and **6a-e**, the Zn(II) complexes of **6b-d**, and of the reference compounds **4**, **5** in CH₂Cl₂.

Cmpd	λ_{abs} (arm) (nm)	λ_{abs} (Soret) (nm)	ϵ (Soret) (10 ³ M ⁻¹ cm ⁻¹)	λ_{abs} (Q bands) (nm)	λ_{em} (nm)		$\Phi_{\text{F}}^{\text{a}}$	$\epsilon^{\text{max}} \cdot \Phi_{\text{F}}^{\text{b}}$ (10 ³ M ⁻¹ cm ⁻¹)	Φ_{Δ}^{c}
					Q(0,0)	Q(0,1)			
4	-	419	440	514,548,590,649	652	719	0.11	48.4	0.60
2a	341	432	539	521,560,596,652	662	725	0.22	118.6	0.64
5	272	425	-	519,557,593,649	659	724	0.24	-	nd ^d
6a	-	426	-	519,555,596,652	660	724	0.18	-	0.64
6b	374	435	540	522,562,595,653	663	729	0.22	118.8	0.67
6c	402	437	646	522,562,594,653	663	729	0.22	142.1	0.63
6d	419	443	934	522,562,594,653	663	728	0.22	205.5	0.62
6e	400 / 420	446	1076	521,561,595,653	663	728	0.20	215.2	0.58
6b-Zn	373	437	483	556, 598	612	660	0.09	43.5	0.43
6c-Zn	401	441	857	556, 598	612	660	0.08	68.6	0.55
6d-Zn	415	445	934	556, 599	612	661	0.09	84.1	0.52

^a Fluorescence quantum yield determined relative to TPP (**4**) in toluene ($\Phi_{\text{F}}[\mathbf{4}] = 0.11$).^[22] ^b Brightnesses ($\epsilon^{\text{max}} \cdot \Phi_{\text{F}}$).^[23]

^c Oxygen photosensitization quantum yield determined relative to TPP (**4**) in CH₂Cl₂ ($\Phi_{\Delta}[\mathbf{4}] = 0.60$).^[24] ^d Not determined.

The existence of an energy transfer (ET) process between the peripheral fluorenyl conjugated arms and the central porphyrin core was also probed (Figure 2).^[6b, 9] After excitation of **2a** and **6b** in the arm-centered π - π^* absorption band, the emission spectra show only the red emission (at 660 and 725 nm) of the porphyrin core and almost no residual blue emission of the arm. This implies that the latter is completely quenched through an efficient process that most likely corresponds to ET from the conjugated arm to the porphyrin core in line with previous studies on related derivatives.^[6b, 9] In contrast, the TFP-cored porphyrins **6c-e** which feature longer peripheral arms show two emissions: (i) a red emission (at 660 and 725 nm) similar to that of

2a and **6b** and (ii) a blue emission appearing around 450 nm which corresponds to an arm-based emission, showing that the corresponding $\pi^* \leftarrow \pi$ excited state is not totally quenched by ET in these derivatives. Exploiting the strong fluorescence quantum yields of the fluorenaldehyde precursors **8-11** ($\Phi_F \geq 0.90$), the ET efficiencies of porphyrins **6b-6d** have been estimated (via eq. 1) using **8-11** as energy-donor models (see ESI for more details):

$$\Phi_{\text{EnT}} = 1 - \Phi_{\text{Arms of Porphyrin}} / \Phi_{\text{Aldehyde}} \quad (1)$$

Note that regarding compounds **8-11**, such comparably large fluorescence quantum yields are not uncommon for fluorene derivatives featuring an aldehyde function,^[25] even when a vinyl group is also present on the fluorophore.^[26] Values higher than 90% have been found for all compounds (see ESI, Table S2). Porphyrin **6b** exhibits an ET efficiency of more than 99%, whereas **6e** exhibits the lowest value, which is still 91%. Given that the **TFP**-cored porphyrins **6c-e** feature the longest poly(ethenyl-2,7-fluorenyl) arms, the most peripheral fluorenes are possibly too remote from the porphyrin core to permit the ET process becoming kinetically competitive with arm-based radiative deactivation. This ET most likely corresponds to a so-called “through-bond” energy transfer (TBET) taking place through the pi-manifold,^[27] which starts exhibiting a distance-dependence after sufficient arm extension. This kind of ET is also commonly referred to as Dexter-type energy transfer. At long distances, this process is possibly supplemented by a “through-space” (Förster) ET^[28] which also fails to efficiently quench the arm-based excited state.

Metallated porphyrins. For three zinc(II) complexes of **6b-d**, the UV/Vis absorption spectra and emission spectra were recorded between 250 and 800 nm (Figures 3 and 4 and Table 1). Besides the characteristic features of metallated porphyrins such as (a) the intense Soret-band (435-450 nm) and (b) two Q-band absorptions (560-620 nm), the absorption originating from a π - π^* transition based on the conjugated arms is also observed (370-420 nm). The intensity of

the latter absorption strengthens upon progressing from **6b-Zn** to **6d-Zn** and clear bathochromic shifts are observed for this and for the Soret band upon extension of the peripheral arms, suggesting again the existence of a significant conjugation through the arm-localized π manifold and a more modest one with the porphyrin core.

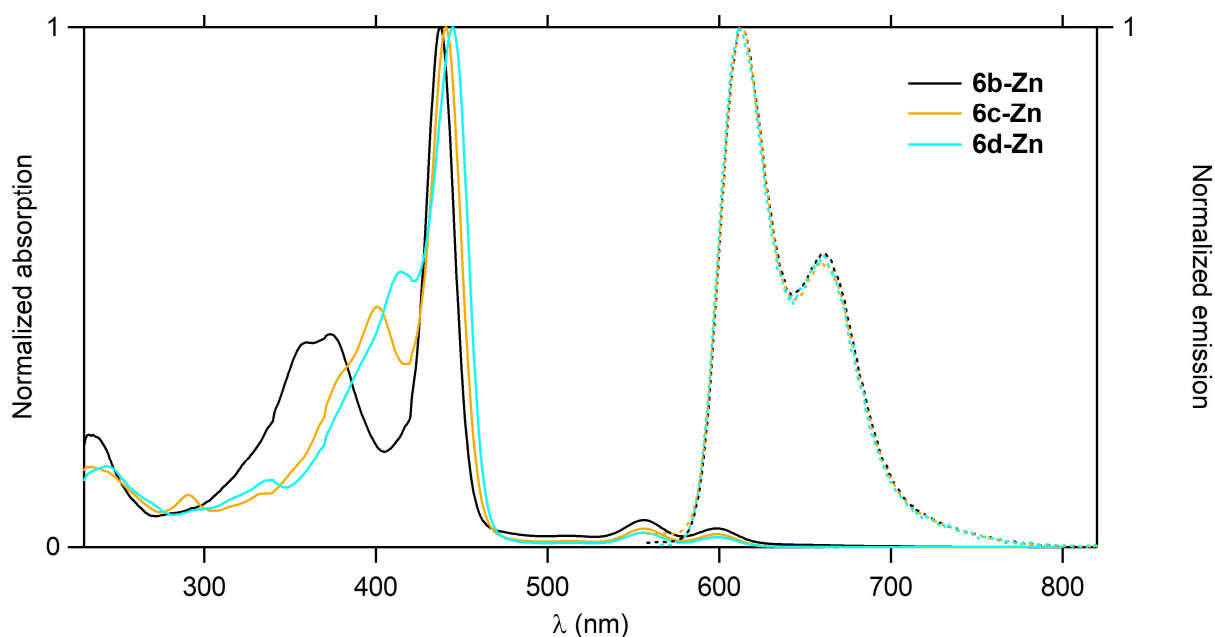


Figure 3. UV-visible absorption and emission spectra of zinc complexes **6b-d-Zn** in CH_2Cl_2 .

Expectedly, due to the occurrence of faster intersystem crossing stimulated by the presence of Zn(II) (heavy atom effect), the fluorescence quantum yields of these compounds are much weaker than for the corresponding free bases. Upon excitation in the arm-centered π - π^* band, all show some residual arm-based emission (Figure 4). Their ET efficiencies (97-98%) are similar to those of the corresponding free bases (see ESI, Table S2), but the residual emission looks more intense in comparison with the porphyrin band, because the fluorescence quantum yield of the zinc complexes is lower than those of the free bases. More surprisingly, in spite of a presumably faster intersystem crossing for Zn(II) complexes, the oxygen photosensitization

yields also decrease compared to those of the corresponding free-bases, suggesting that nonradiative competitive processes repopulating the GS are also faster for the complexes, as already observed for **4** and **4-Zn**.^[17, 29]

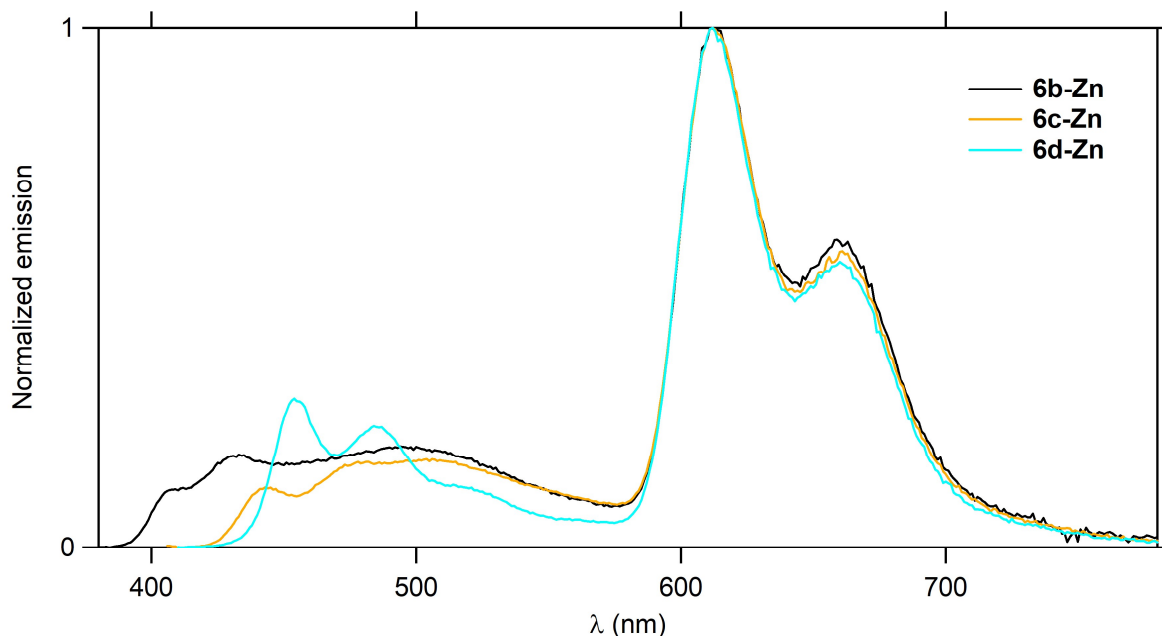


Figure 4. Emission spectra of the zinc complexes **6b-d-Zn** in CH_2Cl_2 upon excitation of the arm-centered $\pi\text{-}\pi^*$ band.

One-photon fluorescence imaging and PDT. Based on one-photon brightness ($\epsilon^{\text{max}} \cdot \Phi_{\text{F}}$),^[23] the largest cross-shaped TFP derivative **6e**, which presents the strongest Soret band and a comparably good fluorescence yield (20%), appears as the most suited compound for performing one-photon fluorescence imaging. Regarding oxygen photosensitization, the new free-base porphyrins **2a** and **6b-e** present rather close Φ_{Δ} quantum yields (58-67 %) which roughly compare to those of reference compounds **4** and **6a** (60% and 64%, respectively), while the corresponding zinc complexes exhibit significantly lower values (43-55%). Thus, contrary to complexation with Zn(II), peripheral extension does not adversely affect the oxygen-photosensitizing capability of these compounds.

Two-photon absorption. The two-photon absorption (2PA) cross-sections were determined by measuring their two-photon excited fluorescence (TPEF) in solution (10^{-4} M) in the femtosecond regime (Figure 5 and Table 2). For most compounds except **6e**, 2PA absorption takes place in a shallow maximum located at slightly higher energy than the Soret band (see ESI; Figure S40). Notably, a fully quadratic dependence of the fluorescence intensity on the excitation power is observed at all wavelengths probed (ESI, Figures S41-42), indicating that the cross-sections (σ_2) are entirely due to 2PA. The **TPP**- and **TFP**-cored compounds exhibit much larger 2PA σ_2 values than **4** and **6a** (12 and 140 GM, respectively). Comparison between **TPP**- (**2a**) and **TFP**-cored (**6b**) free bases reveals that replacing the four *meso*-phenyl groups by four 2-fluorenyl ones leads to a clear improvement of the maximum 2PA cross-section: σ_2^{\max} increases from 700 to 920 GM when going from **2a** to **6b**. Within the **TFP**-cored series, increasing the number of fluorenyl units in the conjugated arms leads to a continuous increase of the 2PA cross-sections, suggesting that conjugation through the 1,2-ethenyl connectors is promoting σ_2^{\max} . As a result, the two-photon cross-sections at lowest energy rises upon going from **6b** to **6e** (from 920 to 2890 GM, respectively). Finally, the data gathered for **6b** to **6d-Zn** reveals that, with these porphyrins, the effect of metallation by Zn(II) is not always similar on 2PA. A 30% decrease on σ_2^{\max} is stated for the shortest compound (**6b-Zn**), while a 45% increase is observed for **6c-Zn** and a smaller increase (5%) for the largest one (**6d-Zn**). Considering the experimental uncertainty on these values ($\pm 10\%$), only the (opposite) effects stated for **6b-Zn** and **6c-Zn** are significant.

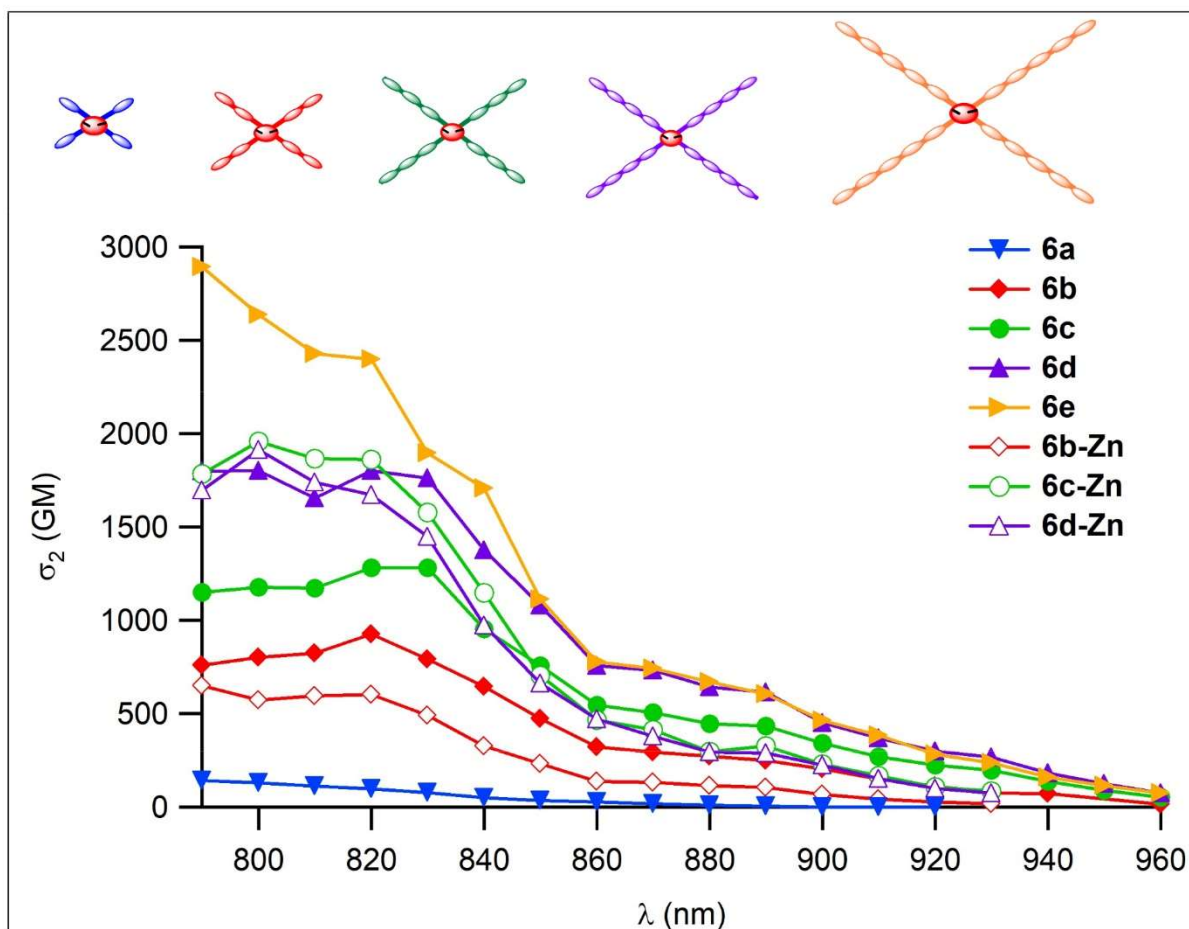


Figure 5. Two-photon absorption spectra of free-base porphyrins (**6a-e**) and some of their zinc complexes (**6b-d-Zn**) in CH_2Cl_2 .

Two-photon fluorescence imaging. When we compare the two-photon action cross-sections ($\sigma_2^{\text{max}} \cdot \Phi_F$) for these compounds, the figure of merit classically used to gauge the performance of a given dye for two-photon fluorescence imaging,^[30] we first notice an increase along the free bases series **6a-e**, thus upon extending the peripheral arms. A similar feature is also observed for the Zn(II) complexes **6b-d**, but, given the large decrease in fluorescence quantum yield after metalation, each of these derivative has a lower action cross-sections than its corresponding free base, even with better σ_2^{max} values. As a result, **6e** has the largest $\sigma_2^{\text{max}} \cdot \Phi_F$ figure of merit (578 GM) and appears to be the best dye for performing two-photon fluorescence imaging. However, when this figure of merit is scaled by the molecular mass M (as an estimate for the

molecular volume), albeit remaining the largest for all **TFP**-cored derivatives tested, it actually compares to that of **2a**. A different statement holds when $\sigma_2^{\max} \cdot \Phi_F$ values are scaled by the squared number of effective electrons (N_e^2).^[31] **2a** now ranks significantly better than any **TFP**-cored series (**6a-e**). Thus, both in terms of molecular design and synthetic effort, the star-shaped porphyrin **2a** appears to be optimal for performing two-photon imaging.

Two-photon PDT. The two-photon efficiency for singlet oxygen generation ($\sigma_2^{\max} \cdot \Phi_\Delta$) is the figure of merit usually used to evaluate the capability of a two-photon absorbing dye to work as a photosensitizer for two-photon PDT applications (Table 2). Among the free-base porphyrins, this figure increases continuously from **2a** to **6e** (448 to 1676 GM), whereas its progression is more erratic for the zinc complexes; it increases strongly from **6b-Zn** to **6c-Zn** (280 to 1078 GM) and then decreases slightly for **6d-Zn** (993 GM). When it is scaled by the molecular mass (M), the best value is now obtained for **6c-Zn**, just above that for **6e** and for **2a**. However, when it is scaled by the squared number of effective electrons (N_e^2), **2a** remains the best compound (0.232 GM) in terms of molecular design, however, closely followed by the fluorenyl-based analog **6b**. Thus, based on synthetic access, the free base **2a** certainly belongs to the most promising two-photon absorbers for photosensitization of oxygen. In terms of specific 2PA efficiency for that task, it is challenged by the Zn(II) complex **6c-Zn**. Thus, complexation by Zn(II) appears as a potential mean to improve further the performances of such free-base porphyrin-based photosensitizers in selected cases. Remarkably, so far, no clear trend can be evidenced between structure and photosensitizing ability for the various Zn(II) complexes presently synthesized (**6b-d-Zn**).

Table 2. Two-photon absorption and two-photon singlet oxygen generation and related figures of merit for free-base (2a, 6a-e) and metallated porphyrins (6b-d-Zn) and for the corresponding reference compounds (4 and 5) in CH₂Cl₂.

Cmpd	λ_{2PA}^{max} (nm)	σ_2^{max} (GM) ^a	σ_2^{max}/N_e^2 (GM) ^b	Φ_F ^c	Φ_Δ ^d	$\sigma_2^{max} \cdot \Phi_F$ (GM) ^e	$\sigma_2^{max} \cdot \Phi_F / N_e^2$ (GM) ^f	$\sigma_2^{max} \cdot \Phi_F / M$ (GM) ^g	$\sigma_2 \cdot \Phi_\Delta^{max}$ (GM) ^h	$\sigma_2 \cdot \Phi_\Delta^{max} / N_e^2$ (GM) ⁱ	$\sigma_2 \cdot \Phi_\Delta^{max} / M$ (GM) ^j
4	790	12	0.025	0.11	0.60	1.3	0.003	0.002	7.2	0.015	0.012
5	790	90	0.099	0.24	0.60	22	0.024	0.022	54	0.060	0.056
2a	820	700	0.362	0.22	0.64	154	0.080	0.084	448	0.232	0.246
6a	790	140	0.154	0.18	0.64	25	0.028	0.018	54	0.099	0.063
6b	820	920	0.303	0.22	0.67	202	0.067	0.077	616	0.203	0.235
6c	830	1280	0.190	0.22	0.63	282	0.042	0.073	806	0.120	0.210
6d	830	1800	0.150	0.22	0.62	396	0.033	0.078	1116	0.093	0.221
6e	790	2890	0.153	0.20	0.58	578	0.031	0.092	1676	0.089	0.268
6b-Zn	790	650	0.214	0.09	0.43	59	0.019	0.022	280	0.092	0.104
6c-Zn	800	1960	0.291	0.08	0.55	157	0.023	0.040	1078	0.160	0.276
6d-Zn	800	1910	0.159	0.09	0.52	172	0.014	0.034	993	0.083	0.194

^a Maximum of the intrinsic 2PA cross-sections measured by TPEF in the femtosecond regime; a fully quadratic dependence of the fluorescence intensity on the excitation power is observed and 2PA responses are fully non-resonant. ^b 2PA cross-sections corrected by the squared effective number of electrons.^[31] ^c Fluorescence quantum yield determined relative to H₂TPP (**4**) in toluene. ^d Singlet oxygen formation quantum yield determined relative to H₂TPP (**4**) in CH₂Cl₂ (Φ_Δ [**4**] = 0.60).^[24] ^e Two-photon brightness (or 2P action cross-section) at the 2PA maximum.^[32] ^f Two-photon brightness corrected by the squared effective number of electrons.^[31] ^g Two-photon brightness corrected for the molecular weight (M) (or specific two-photon brightness). ^h Two-photon efficiency for PDT. ⁱ Two-photon efficiency for PDT corrected by the squared effective number of electrons.^[31] ^j Two-photon efficiency for PDT corrected for the molecular weight (or specific two-photon efficiency for PDT).

Structure-property relationships and applied perspectives for 2a, 6a-e and their Zn(II) complexes. As previously shown, the study of selected one- and two-photon-based photonic properties of the new star-shaped free-base porphyrins **2a**, **6a-e** and of some of their zinc(II) complexes (**6b-d-Zn**) complemented by the analysis of relevant figures of merit allows delineating structure-dependent trends for 2PEF imaging and 2POS. It is now interesting to compare performances of these **new starburst compounds** with those of their **dendrimeric homologues** previous studied in our group, but also with other porphyrin-based systems independently reported in the literature for these tasks. Such an approach will allow to further probe the interest of fully symmetric porphyrins type **A4**, having peripheral arms “semi-disconnected” from the central core for performing PDT and fluorescence imaging.^[33] For such *meso*-tetraarylporphyrins, semi-disconnection automatically results from the tilt angle adopted by the peripheral aryl rings and the porphyrin plane due to steric strain.^[34] As previously shown, this feature allows to keep the linear optical properties of interest of the central core (Soret band absorption and Φ_F) nearly unchanged, while allowing to modify the NLO properties of the compound (2PA) by appropriate structural variations of the peripheral arms.^[5e, 6b, 8-9, 35]

Starburst vs. dendrimeric architectures for promoting 2PA. For the first time with the star-shaped free bases **6a-e**, we show that a continuous increase in σ_2 is achieved by increasing the number of conjugated fluorene units in the arms at the *meso*-positions (Figure 5), while at best a stagnation or (more often) a decrease had been previously observed for increasing generations of dendrimeric homologues such as **1a-c** or **3a-c**.^[6b, 9] From Table 3, it is clear that starburst architectures in which all the peripheral aromatic units are conjugated with the central porphyrin

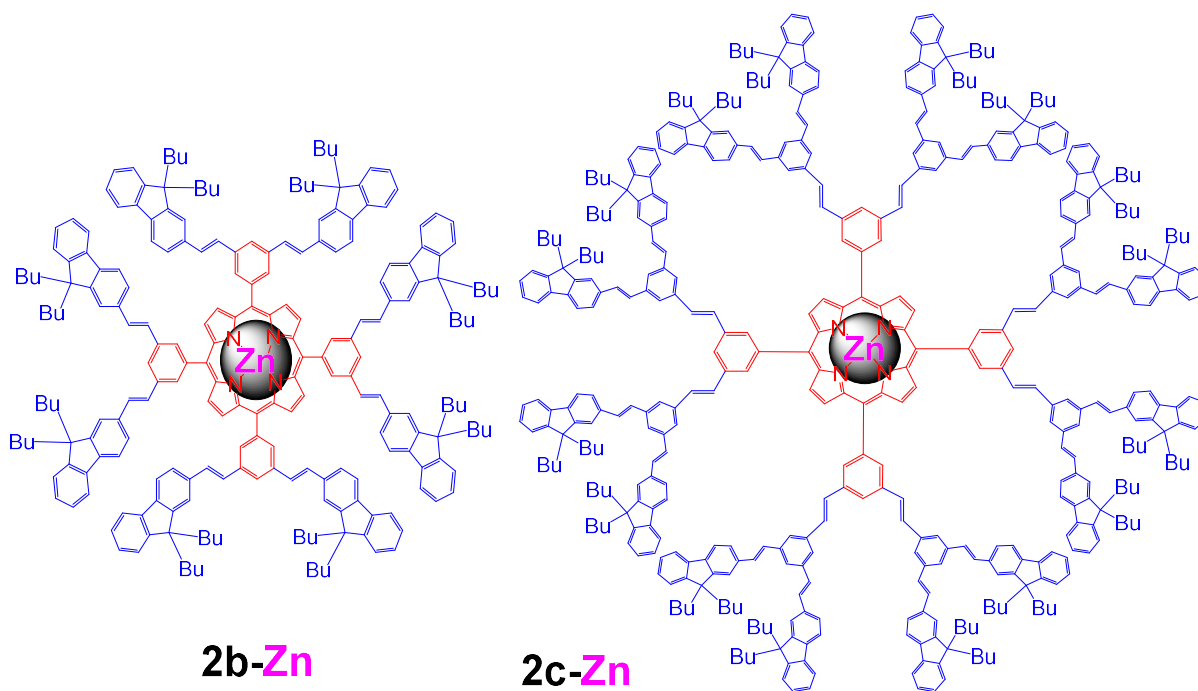
core represent the best design for optimizing the 2PA cross-sections (*e.g.* compare **6b** with **2b**). Then, in line with a statement previously made for dendrimers,^[9] we find again that **TFP**-cored compounds (**6b**) exhibit larger σ_2^{\max} values than their **TPP** homologues (**2a**), a statement which may be related to the total number of 2,7-fluorenyl moieties present at their periphery, since these aromatic units are well known to favor 2PA (and fluorescence) when inserted in well-designed molecular architectures.^[5e, 33] However, considering that a fluorene unit has two time more π -electrons than a phenyl one, in line with a proposal originally made by Kuzyk,^[31, 36] σ_2^{\max} values need to be corrected by the squared number of “effective” π -electrons (N_e^2) to properly estimate the impact of this structural change on 2PA. This reveals that some “saturation”^[37] rapidly takes place with the extension of the peripheral arms when progressing from **6a** to **6e**, but this effect is less marked than when the various π -bonds are not all conjugated together upon extension, as was the case in dendrimers **1a-c** or **3a-c**. Thus, for a given number of fluorene groups, starburst porphyrins **1a**, **2a**, **3a** and **6a-e** are better two-photon absorbers than their dendrimeric analogues and the following ranking emerges between these compounds: **2a** > **6b** > **3a** > **1a**. Among them, the new compound **2a** exhibits the best 2PA response per effective π -electron. In line with independent observations, this ranking also definitively confirms that **1,2-alkene spacers** are better than **1,2-alkyne ones** to promote 2PA, a statement already made for dendrimers^[8] and more general for among two-photon absorbers.^[7b] This effect is most likely related to the better “electronic communication” allowed between aromatic units by these spacers compared to 1,2-alkyne spacers.^[38] Remarkably, the same ranking is observed between **1a**, **3a**, **2a** and **6b** when σ_2^{\max} values are corrected for their molecular mass (M), as an indirect mean to estimate their steric dependence (Table 3). However, with this figure

of merit (σ_2^{\max}/M), the highest values among star-shaped free-base porphyrins is now obtained for **6e** (0.462 GM.mol/g) and not for **2a** (0.384 GM.mol/g), revealing that in spite of the previous saturation effect observed with N_e^2 , the increase in molecular volume when progressing from **2a** to **6e** is more than compensated by the increase in σ_2^{\max} , a useful hint in term of molecular design. Another positive effect for bio-related applications which accompanies the change in geometry from dendrimeric to starburst for a given number of 2,7-fluorene units is the red shift of the overall 2PA peak, which mirrors the increased conjugation of the peripheral arms. In **2a** and **6b-e**, this phenomenon is also dependent on its length (Figure 5). Thus, as long as the 2PA peak remains in the NIR-I region,^[39] this gives some added value to the larger compounds exhibiting comparable 2PA cross-sections. Thus, in contrast to what was previously observed for dendrimer-like systems such as **1a-c** or **3a-c**, increasing the size of the conjugated arms in starburst architectures such as **6a-e** constitute a simple mean to enhance the 2PA response of these semi-disconnected compounds and provide access to more and more active two-photon photosensitizers also adapted to theranostic approaches.

Table 3. Selected biphotonic photophysical properties of TPP- and TFP-cored porphyrins related to 2a, 6b-e and 6b-d-Zn in CH₂Cl₂.

Cmpd	Core/Spacer	n_{Fl}^a	M^b (g/mol)	N_e^c	$\lambda_{2PA}^{max\ d}$ (nm)	$\sigma_2^{max\ e}$ (GM)	σ_2^{max}/M (GM.mol/g)	Φ_F^f	Φ_Δ^g	σ_2^{max}/N_e^2 (GM)	$\sigma_2^{max} \cdot \Phi_F/M$ (GM)	$\sigma_2^{max} \cdot \Phi_\Delta/M$ (GM)
1a	TPP/alkyne	4	1816	45.6	790	380	0.209	0.18	0.70	0.183	0.038	0.146
1b	TPP/alkyne	8	3018	48.0	790	200	0.066	0.12	0.59	0.087	0.008	0.039
2b	TPP/alkene	8	3034	45.2	790	280	0.092	0.13	0.64	0.137	0.012	0.059
2b-Zn^h	TPP/alkene	8	3093	45.2	790	260	0.084	0.03	0.59	0.127	0.003	0.050
2c-Zn^h	TPP/alkene	16	6303	64.2	810	450	0.071	0.06	0.55	0.109	0.004	0.039
3a	TFP/alkyne	8	2618	55.2	790	770	0.294	0.23	0.62	0.253	0.068	0.182
3b	TFP/alkyne	12	4220	59.6	790	730	0.173	0.23	0.61	0.206	0.040	0.106
3c	TFP/alkyne	28	9828	75.6	790	740	0.075	0.22	0.60	0.129	0.017	0.045
2a	TPP/alkene	4	1824	44.0	820	700	0.384	0.22	0.64	0.362	0.084	0.246
6a	TFP/alkene	4	1416	30.1	790	140	0.154	0.18	0.64	0.154	0.018	0.063
6b	TFP/alkene	8	2626	55.1	820	920	0.350	0.22	0.67	0.303	0.077	0.235
6c	TFP/alkene	12	3835	82.0	820	1280	0.333	0.22	0.63	0.190	0.073	0.210
6e	TFP/alkene	20	6255	137.2	790	2890	0.462	0.20	0.58	0.153	0.092	0.268
6c-Zn	TFP/alkene	12	3899	82.0	800	1960	0.502	0.08	0.55	0.291	0.040	0.276

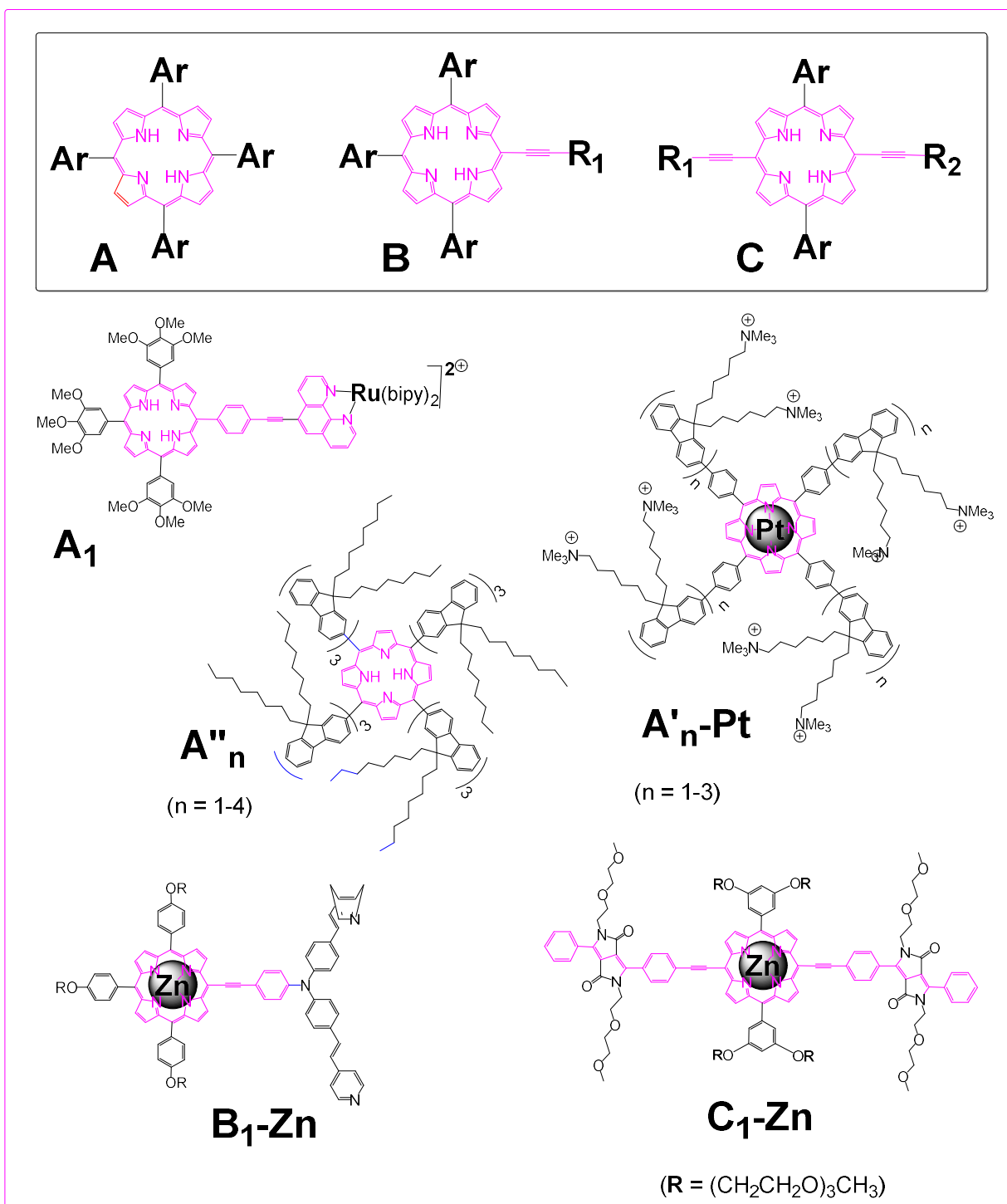
^a Number of fluorene units in the molecule. ^b Molecular weight. ^c Number of effective π -electrons.^[36] Note that this number is presently not changed by metallation, in line with the assumption that the Zn(II) does not contribute to increase the number of effective electrons. ^d Wavelength at the maximum 2PA. ^e Maximum intrinsic 2PA cross-section (TPEF). ^f Fluorescence quantum yield determined relative to H₂TPP (**4**) in toluene. ^g Singlet oxygen formation quantum yield determined relative to TPP (**4**) in dichloromethane ($\Phi_\Delta[\mathbf{4}] = 0.60$).^[24] ^h See Scheme 8.



Scheme 8. Metallated dendrimeric porphyrins previously reported.

Metallation by Zn(II) for promoting 2PA. So far, for such dendrimeric porphyrin-based systems, metallation by Zn(II) had never been identified as a mean to increase their 2PA cross-section compared to the corresponding free base.^[40] Instead, metallation had always had a weakly negative (or insignificant) effect on 2PA, while severely hampering the luminescence, thus appeared as an overall detrimental factor for two-photon theranostics (compare **2b** and **2b-Zn** in Table 3). Presently the same statement can be made for **6b** and **6d**, but not for **6c** for which complexation by Zn(II) allows to strongly increase the 2PA from 1280 to 1960 GM, making **6c-Zn** even more attractive than the largest free-base porphyrin **6e** (see σ_2^{\max}/M values). This is not the case when the 2PA cross-section is scaled by N_e^2 rather than size (M), **2a** remaining the best compound in this case. The origin of the improvement in the 2PA cross-section of **6c-Zn** relative to **6c** cannot be ascertained without computations. However, based on existent knowledge,^[41] this effect might be tentatively be attributed to the increase in symmetry

of the compound after metallation, possibly resulting in more numerous strongly 2PA-allowed (*g*-type) excited states in the vicinity of the Soret band.



Scheme 9. Selected examples of other porphyrin-based photosensitizers independently reported for PDT (in purple, the main π -manifold).

Star-shaped carbon-rich porphyrins for 2PA-fluorescence Imaging and 2PA-PDT. Whereas porphyrin derivatives played a central role as photosensitizers for PDT,^[10a] they were

subsequently envisioned for theranostics^[10b] and eventually adapted for 2PA excitation.^[42] However, among these, only few are actually *meso*-tetraaryl derivatives (**A**) featuring “carbon-rich” peripheral arms (Scheme 9).^[43] To the best of our knowledge, apart for some asymmetric derivatives presenting one extended *meso*-aryl group, such as **A₁** or **A₁-Zn** for instance,^[44] no discrete and well defined *meso*-tetraaryl porphyrins, such as **A'_n** or **A''_n**,^[3d, 14-15, 45] were ever tested as photosensitizers for 2PA-PDT, although related Pt(II) complexes (**A'_n-Pt**) were recently used for one-photon PDT and oxygen quantification.^{[14],[15]} Apart from these few examples, most of the active porphyrin-based 2PA photosensitizers are Zn(II) complexes, for which one (**B**) or two (**C**) *meso*-aryl ring(s) have been replaced by extended arylalkynyl ligand(s),^[42, 46] a structural modification which allows better conjugation of the central π -manifold with the peripheral arms, because not disrupted by any tilt angle. The net result of this “extension” of the porphyrin central core is to improve its number of effective electrons (N_e) and, in turn, to significantly increase the 2PA cross-section,^[37] but also to significantly complicate the synthesis of the compound. This structural modification also red-shifts the Q-bands and increases their intensity, shifting to higher wavelengths the high-energy border of the 2PA window, as observed with **B₁**^[47] or **C₁-Zn**,^[48] an effect which can sometimes become limitative from a practical standpoint, especially when the region between the first and second NIR windows (900-1000 nm) is reached.^[39, 49]

Now, considering that the fluorescence quantum yield of all free-base starburst compounds ever studied in our group (**1a**, **2a**, **3a**, **6a-e**) remains comprised between 0.18-0.24 in CH₂Cl₂ (Table 2) and that the oxygen photosensitization yield remains comprised in between 0.58-0.64 (and is 0.70 only for **1a**), we see that once vectorization has been properly addressed,^[13] it is mostly

the change of their 2PA properties that will decide of their interest for performing 2PA fluorescence imaging or PDT. In this respect, although the performances of the model compounds **2a**, **6b** or **6e** appear inferior to those of the best C-type porphyrin dimers designed so far,^[46] they stand comparison with those of many mono-porphyrin derivatives such as **B1**^[47] or **C1-Zn**^[50] (Scheme 9) and largely exceed those available for common *meso*-tetraaryl derivatives (Table 4), making starburst compound interesting photosensitizers. As presently observed for **6b-d** and also independently exemplified by the data reported **A'3-Pt** and **A''3**,^[3d, 14] metalation usually strongly depresses the emission quantum yield of the porphyrin, reviving the interest of free bases for theranostic approaches. Furthermore, as mentioned above, these symmetric compounds are often easier to access synthetically than non-symmetric porphyrins (belonging to the **B** or **C** types). Finally, considering that structural parameters conditioning the efficiency of such photosensitizers is still poorly understood,^[43] and given that their internalization and intra-cell localization can be largely determined by small changes in size or structure,^[13a] the possibility of using a large set of compounds with overall good figures of merit but with very diverse size and structures, such as **2a**, **6b**, **6e** and **6c-Zn**, significantly improves the chances of identifying an active photosensitizer for a given cancer type.

Table 4. Comparison of 2a, 6b, 6e and 6c-Zn with selected porphyrin-based photosensitizers reported in the literature. ^a

Cmpd	n_{FI}	M (g/mol)	N_e	<i>Solvent</i>	λ_{2PA}^{max} (nm)	σ_2^{max} (GM)	σ_2^{max}/M (GM.mol/g)	Φ_F	Φ_Δ	σ_2^{max}/N_e^2 (GM)	$\sigma_2^{max} \cdot \Phi_F/M$ (GM)	$\sigma_2^{max} \cdot \Phi_\Delta/M$ (GM)
2a	4	1824	44.0	CH ₂ Cl ₂	820	700	0.384	0.22	0.64	0.362	0.084	0.246
6b	8	2626	55.1	CH ₂ Cl ₂	820	920	0.350	0.22	0.67	0.303	0.077	0.235
6e	20	6255	137.2	CH ₂ Cl ₂	790	2890	0.462	0.20	0.58	0.153	0.092	0.268
6c-Zn	12	3899	82.0	CH ₂ Cl ₂	800	1960	0.502	0.08	0.55	0.291	0.040	0.276
A₁	0	1500	41.5	DMSO	800 ^b	168 ^b	0.112	0.05	0.58	0.098	0.006	0.065
A₁-Zn	0	1563	41.5	DMSO	800 ^b	228 ^b	0.146	0.003	0.73	0.132	0.000	0.106
A''₃	12	4974	74.3	toluene	nd ^c	nd ^c	/	0.19	nd ^c	/	/	/
A''₃-Pt	12	7202	84.9	H ₂ O ^d	nd ^c	nd ^c	/	0.03	0.92	/	/	/
B₁-Zn	0	1559	34.5	DMSO	830	317	0.203	0.03	0.74 ^e	0.266	0.006	0.150
C₁-Zn	0	2204	55.0	DMSO	910	935	0.424	0.19	0.51	0.309	0.081	0.216

^a Headings of the Table have their usual meaning (see Table 3). ^b Not a 2PA maximum. ^c Not determined. ^d Determined in degassed H₂O. ^e Determined in DMF.

Conclusions

Series of new star-shaped free-base porphyrins (**2a**, **6b-e**) including 2,7-fluorenyl units in their peripheral conjugated arms as well as their zinc(II) complexes (**6b-d-Zn**) have been synthesized and characterized. Their emission properties, 2PA and photosensitizing ability toward oxygen were measured and clear structural-dependent trends have been delineated. First, we show that extension of the conjugated peripheral arms constitutes a simple means to increase 2PA of these free-base porphyrins. Second, we establish that this structural change affects only marginally their fluorescence and their photosensitizing quantum yields, in line with expectations based their “semi-disconnected” structure. Analysis of relevant figures of merit further indicates that the shorter free bases among them (**2a**) are likely to be the most promising compounds for developing water-soluble dyes for theranostic approaches either from the standpoint of synthetic effort or efficacy. However, in the case of 2PA-PDT alone, the most extended compounds remain competitive with the shorter free-bases. In this respect, *a contrario* to observations previously made in related dendrimeric families, metallation by Zn(II) can allow a further improvement of their oxygen photosensitizing ability. This unexpected observation appears however to be very compound-specific and currently escapes any simple rationalization.

Thus, whereas we had previously shown that (i) increasing the dendrimeric generation was a mean to increase the 2PA cross-section for porphyrin-centered dendrimers containing 2,7-fluorenyl units in their dendrons, without affecting significantly the fluorescence quantum yield (Φ_F), that (ii) carbon-rich dendrons featuring conjugated segments (Scheme 1) were much more effective than phenoxyether-containing ones for promoting 2PA, that (iii) **1,2-alkene linkers**

were better suited as connectors for that task than **1,2-alkyne** ones and that (iv) **TFP**-cored dendrimers, due to their increased luminescence and larger 2PA cross-section, were also better-suited than their **TPP** analogues, we now demonstrate that, (v) for a given number of fluorene units in the peripheral arms, **star-shaped architectures** outperform dendritic ones. In addition, the photonic performances of **2a**, **6b**, **6e** or **6c-Zn** appear clearly above those of many *meso*-tetraaryl porphyrins independently reported in the literature for two-photon-based cancer treatment or imaging. Thus, given their diversity in size, these new compounds remarkably enrich the existing library of two-photon photosensitizers potentially usable for PDT. So far, we have already shown that they might be vectorized in cells, either *via* inclusion in *ad hoc* biocompatible nanoparticles or after proper chemical functionalization allowing to water-solubilize them. Thus, these results are very encouraging to explore further the applied potential of these fascinating compounds for theranostics or related medical uses. Work along these lines is currently in progress in our group.

Experimental Section

General

Compounds were purified by chromatography on silica gel using different mixtures of eluents as specified. Unless otherwise stated, all solvents used in reactions were distilled using common purification protocols,^[51] except DMF and ⁱPr₂NH which were dried on molecular sieves (3 Å). ¹H and ¹³C NMR spectra were recorded on Bruker ASCEND 400 and ASCEND 500 at 298 K. The chemical shifts are referenced to internal tetramethylsilane (TMS). High-resolution mass

spectra were recorded on different spectrometers: a Bruker MicrOTOF-Q II, a Thermo Fisher Scientific Q-Exactive in ESI positive mode and a Bruker Ultraflex III MALDI Spectrometer at CRMPO (Centre Regional de Mesures Physiques de l'Ouest) in Rennes. Reagents were purchased from commercial suppliers and used as received. The phosphonate **12** and the aldehyde **13** were obtained using procedures previously described in the literature.^[9, 20] The synthesis of precursor **20** is given in the ESI.

Starburst porphyrin synthesis

TPP-cored porphyrin (2a). In a Schlenk tube, boron trifluoride etherate (21 μ L) was added to a solution of benzaldehyde **7** (275 mg, 0.67 mmol, 1 eq) and pyrrole (49 μ L, 0.67 mmol, 1 eq) in CHCl_3 (20 mL) under argon atmosphere, the reaction was stirred for 4 hours at room temperature. DDQ (113.9 mg, 0.50 mmol, 75% eq) was added and stirring was continued for an additional hour. The solvent was evaporated and the residue was purified by column chromatography (heptane/ CH_2Cl_2 = 3/1, vol/vol), leading to porphyrin **2a** as a purple powder (110 mg, 36%). ^1H NMR (300 MHz, CDCl_3 , ppm): δ 8.98 (s, 8H), 8.28 (d, J = 7.8 Hz, 8H), 7.97 (d, J = 8.1 Hz, 8H), 7.79 (t, J = 7.8 Hz, 8H), 7.69 (d, J = 9.0 Hz, 8H), 7.56 (dd, J = 18.9, 16.5 Hz, 8H), 7.42-7.34 (m, 12H), 2.10 (t, J = 8.1 Hz, 16H), 1.24-1.12 (m, 16H), 0.79-0.70 (m, 40H), -2.61 (s, 2H). $^{13}\text{C}\{^1\text{H}\}$ NMR (75 MHz, CDCl_3 , ppm): δ 151.4, 151.1, 141.3, 141.2, 140.8, 137.0, 136.3, 135.1, 130.3, 127.6, 127.1, 126.8, 124.8, 122.9, 121.0, 120.0, 119.7, 55.0, 40.3, 26.0, 23.1, 13.9. HRMS-MALDI: m/z calcd for $\text{C}_{136}\text{H}_{134}\text{N}_4$: 1823.0608; $[\text{M}]^+$; found: 1823.0430. Anal. Calcd. (%) for $\text{C}_{136}\text{H}_{134}\text{N}_4 \bullet \text{CH}_2\text{Cl}_2$: C, 86.17; H, 7.18; N, 2.93. Found: C, 86.66; H, 7.20; N, 2.91.

TFP-cored porphyrin (6b). In a Schlenk tube, boron trifluoride etherate (15.5 μL) was added to a solution of fluorenaldehyde **8** (300 mg, 0.49 mmol, 1 eq) and pyrrole (36 μL , 0.49 mmol, 1 eq) in CHCl_3 (15 mL) under argon atmosphere. The solution was stirred for 4 hours at room temperature. DDQ (84 mg, 0.37 mmol, 75% eq) was added and stirring was continued for an additional hour. The solvent was evaporated and the residue was purified by column chromatography (heptane/ CH_2Cl_2 = 1/1, vol/vol), leading to **6b** as a purple powder (145 mg, 45%). ^1H NMR (300 MHz, CDCl_3 , ppm): δ 8.98 (s, 8H), 8.31-8.23 (m, 8H), 8.12 (d, J = 7.5 Hz, 4H), 7.99 (d, J = 7.8 Hz, 4H), 7.81-7.71 (m, 16H), 7.62 (d, J = 8.1 Hz, 8H), 7.46-7.32 (m, 20H), 2.23 (s, 16H), 2.07 (t, J = 8.1 Hz, 16H), 1.29-1.09 (m, 32H), 1.08-0.92 (m, 16H), 0.82 (dd, J = 13.8, 6.9 Hz, 24H), 0.76-0.61 (m, 40H), -2.49 (s, 2H). ^{13}C $\{^1\text{H}\}$ NMR (75 MHz, CDCl_3 , ppm): δ 151.3, 151.0, 141.0, 140.9, 136.9, 136.5, 133.8, 133.2, 130.6, 128.9, 128.6, 127.1, 126.8, 125.9, 125.6, 122.9, 120.9, 120.8, 120.7, 119.9, 119.7, 55.3, 55.0, 40.5, 26.0, 23.2, 23.1, 14.1, 14.0, 13.9, 13.8. HRMS-MALDI: m/z calcd for $\text{C}_{196}\text{H}_{214}\text{N}_4$: 2623.687; $[\text{M}]^+$; found: 2623.8217. Anal. Calcd. (%) for $\text{C}_{196}\text{H}_{214}\text{N}_4$: C, 89.65; H, 8.21; N, 2.13. Found: C, 88.27; H, 8.25; N, 2.04.

TFP-cored porphyrin (6c). In a Schlenk tube, boron trifluoride etherate (10 μL) was added to a solution of fluorenaldehyde **9** (290 mg, 0.32 mmol, 1 eq) and pyrrole (23 μL , 0.32 mmol, 1 eq) in CHCl_3 (20 mL) under argon atmosphere. The solution was stirred for 4 hours at room temperature. DDQ (54 mg, 0.24 mmol, 75% eq) was added and stirring was continued for an additional hour. The solvent was evaporated and the residue was purified by column chromatography (heptane/ CH_2Cl_2 = 1/1, vol/vol), leading to **6c** as a purple powder (142 mg, 39%). ^1H NMR (300 MHz, CDCl_3 , ppm): δ = 8.98 (s, 8H), 8.30-8.22 (m, 8H), 8.11 (d, J = 7.3

Hz, 4H), 7.99 (d, $J = 7.9$ Hz, 4H), 7.75-7.71 (m, 26H), 7.63-7.56 (m, 18H), 7.40-7.32 (m, 32H), 2.22-2.01 (m, 48H), 1.30-1.14 (m, 48H), 0.84-0.68 (m, 120H), -2.49 (s, 2H). $^{13}\text{C}\{^1\text{H}\}$ NMR (75 MHz, CDCl_3 , ppm): $\delta = 151.6, 151.3, 151.0, 141.0, 140.9, 140.8, 136.6, 136.5, 128.7, 128.6, 127.0, 126.8, 125.8, 125.6, 122.9, 120.7, 120.0, 55.0, 40.5, 40.4, 26.0, 23.2, 23.1, 14.1, 14.0, 13.9, 13.8$. HRMS-MALDI: m/z calcd for $\text{C}_{288}\text{H}_{318}\text{N}_4$: 3832.501; $[\text{M}]^+$; found: 3832.222. Anal. Calcd. (%) for $\text{C}_{288}\text{H}_{318}\text{N}_4 \bullet \text{CH}_2\text{Cl}_2$: C, 88.54; H, 8.23; N, 1.43. Found: C, 87.77; H, 8.30; N, 1.47.

TFP-cored porphyrin (6d). In a Schlenk tube, boron trifluoride etherate (5.7 μL) was added to a solution of fluorenaldehyde **10** (220 mg, 0.18 mmol, 1 eq) and pyrrole (13 μL , 0.18 mmol, 1 eq) in CHCl_3 (15 mL) under argon atmosphere. The reaction was stirred for 4 hours at room temperature. DDQ (31 mg, 0.14 mmol, 75% eq) was added and stirring was continued for an additional hour. The solvent was evaporated and the residue was purified by column chromatography (heptane/ $\text{CH}_2\text{Cl}_2 = 1/1$, vol/vol), leading to **6d** as a purple powder (62 mg, 27%). ^1H NMR (300 MHz, CDCl_3 , ppm): $\delta = 8.96$ (s, 8H), 8.32-8.19 (m, 8H), 8.08 (d, $J = 8.0$ Hz, 4H), 7.96 (d, $J = 7.9$ Hz, 4H), 7.74-7.69 (m, 32H), 7.62-7.54 (m, 40H), 7.39-7.29 (m, 36H), 2.23-2.00 (m, 64H), 1.28-1.04 (m, 64H), 0.80-0.63 (m, 160H), -2.52 (s, 2H). $^{13}\text{C}\{^1\text{H}\}$ NMR (75 MHz, CDCl_3 , ppm): $\delta = 151.6, 151.3, 151.2, 151.0, 141.0, 140.9, 140.7, 140.6, 136.5, 128.9, 127.0, 125.8, 125.7, 122.9, 120.7, 119.9, 119.7, 55.0, 40.6, 40.4, 26.0, 23.2, 23.1, 14.1, 14.0, 13.9, 13.8$. HRMS-MALDI: m/z calcd for $\text{C}_{380}\text{H}_{422}\text{N}_4$: 5042.3173; $[\text{M}]^+$; found: 5042.392. Anal. Calcd. (%) for $\text{C}_{380}\text{H}_{422}\text{N}_4 \bullet 2\text{CH}_2\text{Cl}_2$: C, 87.97; H, 8.23; N, 1.07. Found: C, 87.60; H, 8.22; N, 1.13.

TFP-cored porphyrin (6e). In a Schlenk tube, boron trifluoride etherate (2.7 μL) was added to

a solution of fluorenaldehyde **11** (130 mg, 0.086 mmol, 1 eq) and pyrrole (6.3 μ L, 0.086 mmol, 1 eq) in CHCl_3 (15 mL) under argon atmosphere. The reaction was stirred for 4 hours at room temperature. DDQ (14.7 mg, 0.065 mmol, 75% eq) was added and stirring was continued for an additional hour. The solvent was evaporated and the residue was purified by column chromatography (heptane/ CH_2Cl_2 = 1/1, vol/vol), leading to porphyrin **6e** as a purple powder (36 mg, 27%). ^1H NMR (400 MHz, CDCl_3 , ppm): δ = 8.96 (s, 8H), 8.27-8.21 (m, 8H), 8.10-8.09 (m, 4H), 7.98-7.96 (m, 4H), 7.71-7.54 (m, 116H), 7.39-7.29 (m, 24H), 2.21-2.00 (m, 80H), 1.26-1.03 (m, 80H), 0.80-0.57 (m, 200H), -2.54 (s, 2H). $^{13}\text{C}\{^1\text{H}\}$ NMR (100 MHz, CDCl_3 , ppm): δ 151.6, 151.3, 151.0, 140.9, 140.7, 136.5, 128.6, 127.0, 126.8, 125.7, 125.6, 122.9, 120.7, 119.9, 119.7, 55.3, 55.0, 40.6, 40.4, 26.0, 23.2, 23.1, 14.1, 14.0, 13.9. HRMS-MALDI: m/z calcd for $\text{C}_{472}\text{H}_{527}\text{N}_4$: 6251.1361; $[\text{M}+\text{H}]^+$; found: 6251.0720. Anal. Calcd. (%) for $\text{C}_{472}\text{H}_{526}\text{N}_4$: C, 90.63; H, 8.48; N, 0.90. Found: C, 89.11; H, 8.40; N, 0.90.

Zinc(II) porphyrin synthesis

Zinc porphyrin (6b-Zn). Compound **6b** (130 mg, 0.05 mmol, 1 eq) and anhydrous $\text{Zn}(\text{OAc})_2$ (55 mg, 0.30 mmol, 6 eq) were dissolved in CH_2Cl_2 (12 mL) and MeOH (5 mL). The mixture was stirred overnight at 45 $^\circ\text{C}$ under argon atmosphere. The solvents were evaporated and the residue was further purified by recrystallization ($\text{CH}_2\text{Cl}_2/\text{MeOH}$ = 1/15-20, vol/vol), leading to the title compound as a red powder (121 mg, 91%). ^1H NMR (300 MHz, CDCl_3 , ppm): δ 9.06 (s, 8H), 8.26-8.22 (m, 8H), 8.07 (d, J = 6.8 Hz, 4H), 7.95 (d, J = 8.2 Hz, 4H), 7.74-7.58 (m, 24H), 7.37-7.30 (m, 20H), 2.19 (s, 16H), 2.06-2.02 (m, 16H), 1.26-1.08 (m, 32H), 0.80-0.68 (m, 80H). $^{13}\text{C}\{^1\text{H}\}$ NMR (100 MHz, CDCl_3 , ppm): δ 151.3, 151.0, 150.5, 141.6, 141.0, 140.9,

140.3, 137.1, 136.9, 136.5, 133.7, 133.6, 132.0, 129.3, 128.9, 128.6, 127.1, 126.8, 126.0, 125.9, 126.0, 125.7, 122.9, 121.9, 120.9, 120.8, 120.4, 119.9, 119.7, 55.3, 55.0, 40.5, 40.4, 26.0, 23.2, 23.1, 14.1, 14.0, 13.9. HRMS-MALDI: m/z calcd for $C_{196}H_{212}N_4Zn$: 2685.6003; $[M]^+$; found: 2685.021. Anal. Calcd. (%) for $C_{196}H_{212}N_4Zn \cdot 2CH_2Cl_2$: C, 83.18; H, 7.62; N, 1.96. Found: C, 83.53; H, 7.92; N, 1.89.

Zinc porphyrin (6c-Zn). Free-base porphyrin **6c** (120 mg, 0.031 mmol, 1 eq) and anhydrous $Zn(OAc)_2$ (34.5 mg, 0.19 mmol, 6 eq) were dissolved in CH_2Cl_2 (12 mL) and MeOH (6 mL). The solution was stirred overnight at 45 °C under argon atmosphere. The solvents were evaporated and the residue was further purified by recrystallization ($CH_2Cl_2/MeOH = 1/15-20$, vol/vol), providing the title compound as a red powder (109 mg, 89%). 1H NMR (300 MHz, $CDCl_3$, ppm): $\delta = 9.07$ (large s, 8H), 8.34-8.27 (m, 8H), 8.09 (d, $J = 6.9$ Hz, 4H), 7.97 (d, $J = 6.7$ Hz, 4H), 7.72-7.55 (m, 44H), 7.39-7.28 (m, 32H), 2.21-2.06 (m, 48H), 1.38-0.99 (m, 48H), 0.81-0.70 (m, 120H). $^{13}C\{^1H\}$ NMR (75 MHz, $CDCl_3$, ppm): δ 151.9, 151.6, 151.3, 151.0, 141.6, 140.9, 140.8, 140.7, 140.6, 136.6, 136.5, 130.6, 129.3, 128.9, 128.7, 127.1, 127.0, 126.8, 126.0, 125.8, 125.6, 122.9, 122.8, 121.9, 120.9, 120.8, 120.7, 112.0, 119.9, 119.6, 55.3, 55.0, 40.6, 40.4, 26.4, 26.0, 25.9, 23.2, 23.1, 14.1, 14.0, 13.9, 13.8. HRMS-MALDI: m/z calcd for $C_{288}H_{316}N_4Zn$: 3894.4136; $[M]^+$; found: 3894.4340. Anal. Calcd. (%) for $C_{288}H_{316}N_4Zn \cdot H_2O$: C, 88.14; H, 8.00; N, 1.42. Found: C, 87.57; H, 8.07; N, 1.41.

Zinc porphyrin (6d-Zn). Free-base porphyrin **6d** (30 mg, 0.006 mmol, 1 eq) and anhydrous $Zn(OAc)_2$ (6.6 mg, 0.036 mmol, 6 eq) were dissolved in CH_2Cl_2 (12 mL) and MeOH (6 mL). The mixture was stirred overnight at 45 °C under argon atmosphere. The solvents were evaporated and the residue was further purified by recrystallization ($CH_2Cl_2/MeOH = 1/15-20$,

vol/vol), leading to the title compound as a red powder (26 mg, 86%). ¹H NMR (300 MHz, CDCl₃, ppm): δ 9.07 (large s, 8H), 8.34-8.25 (m, 8H), 8.09 (d, *J* = 7.0 Hz, 4H), 7.98 (d, *J* = 6.6 Hz, 4H), 7.85-7.55 (m, 72H), 7.39-7.30 (m, 36H), 2.25-1.94 (m, 64H), 1.26-1.01 (m, 64H), 0.88-0.55 (m, 160H). ¹³C {¹H} NMR (75 MHz, CDCl₃, ppm): δ = 151.9, 151.8, 151.7, 151.6, 150.9, 140.9, 140.7, 140.6, 136.7, 136.6, 128.7, 128.6, 127.0, 126.9, 126.8, 126.1, 125.8, 125.7, 125.6, 122.9, 120.9, 120.8, 120.7, 120.1, 120.0, 112.0, 119.9, 55.3, 55.1, 55.0, 40.8, 40.7, 40.6, 40.5, 40.4, 40.3, 40.3, 26.1, 26.0, 25.9, 25.8, 23.2, 23.1, 14.1, 14.0, 13.9, 13.8. HRMS-MALDI: *m/z* calcd for C₃₈₀H₄₂₀N₄Zn : 5104.2308; [M]⁺; found: 5104.427. Anal. Calcd. (%) for C₃₈₀H₄₂₀N₄Zn•8CH₂Cl₂: C, 80.51; H, 7.59; N, 0.97. Found: C, 80.18; H, 7.42; N, 1.08.

Synthesis of aldehyde precursors

(E)-4-(2-(9,9-Dibutyl-9H-fluoren-2-yl)vinyl)benzaldehyde (**7**). In a Schlenk tube, *n*-BuLi (1.1 mL, 1.74 mmol, 1 eq) was slowly added to a solution of compound **14** (800 mg, 1.74 mmol, 1 eq) in dry THF (60 mL) at -78 °C under argon stream. Stirring was kept at -78 °C for 1 h, then dry DMF (0.5 mL) was added and stirring was maintained at -78 °C for 1 hour. The solution was allowed to warm up to room temperature, and the reaction was stirred for 2 h. Saturated NH₄Cl (aq) was added and the mixture was extracted with ethyl acetate. The combined organic layers were dried over anhydrous Na₂SO₄, filtered and evaporated. The residue was further purified by chromatography (petroleum ether/ethyl acetate = 7/2, vol/vol), leading to the title compound as a yellow solid (539 mg, 76%). ¹H NMR (300 MHz, CDCl₃, ppm): δ = 10.03 (s, 1H), 7.91 (d, *J* = 8.4 Hz, 2H), 7.75-7.70 (m, 4H), 7.58-7.54 (m, 2H), 7.43-7.20 (m, 5H), 2.04 (t, *J* = 8.4 Hz, 4H), 1.18-1.06 (m, 4H), 0.73-0.60 (m, 10H). ¹³C {¹H} NMR (75 MHz, CDCl₃, ppm):

δ 191.5, 151.4, 151.1, 150.8, 150.7, 144.1, 143.7, 140.8, 140.6, 135.4, 134.7, 133.7, 132.9, 130.3, 128.4, 127.8, 127.2, 126.8, 123.2, 122.9, 119.8, 55.0, 40.3, 26.0, 23.1, 13.8. HRMS-ESI: m/z calcd for $C_{30}H_{32}ONa$: 431.23454; $[M+Na]^+$; found: 431.234; calcd for $C_{30}H_{32}OK$: 447.20847; $[M+K]^+$; found: 447.2076. Anal. Calcd. (%) for $C_{30}H_{32}O$: C, 88.19; H, 7.89. Found: C, 87.91; H, 7.83.

(E)-2-(4-Bromostyryl)-9,9-dibutyl-9H-fluorene (14). In a Schlenk tube, a solution of compound **12** (994 mg, 2.97 mmol, 1 eq) and previously prepared 9,9-dibutyl-9H-fluorene-2-carbaldehyde **13** (1.0 g, 3.26 mmol, 1.1 eq) in THF (10 mL) was added to a solution of *t*-BuOK (1.3 g, 11.90 mmol, 4 eq) in dry THF (20 mL) at 0 °C under an argon stream. Stirring was kept at 0 °C for 1 h. The cooling bath was removed, saturated NH_4Cl (aq) was added and the mixture was extracted with ethyl acetate. The combined organic layers were dried over anhydrous Na_2SO_4 , filtered and evaporated. The residue was further purified by chromatography (heptane/ CH_2Cl_2 = 8/1, vol/vol), affording **14** as a white solid (1.3 g, 89%). 1H NMR (300 MHz, $CDCl_3$, ppm): δ = 7.73-7.69 (m, 2H), 7.53 (s, 1H), 7.51-7.49 (m, 3H), 7.46-7.42 (m, 2H), 7.39-7.32 (m, 3H), 7.17 (dd, J = 34.2, 16.5 Hz, 2H), 2.02 (t, J = 8.4 Hz, 4H), 1.17-1.05 (m, 4H), 0.70 (t, J = 7.2 Hz, 6H), 0.67-0.57 (m, 4H).

Diisopropyl ((7-bromo-9,9-dibutyl-9H-fluoren-2-yl)methyl)phosphonate (15). In a Schlenk tube, 2-bromo-7-(bromomethyl)-9,9-dibutyl-9H-fluorene **20** (1.9 g, 4.11 mmol) and triisopropyl phosphite (5.6 mL) were successively added under an argon stream. The reaction was refluxed for 3 h at 65 °C. The excess of triisopropyl phosphite was removed under reduced pressure. Then the product was purified by chromatography (CH_2Cl_2), giving **15** as a white solid (2.0 g, 90%). 1H NMR (300 MHz, $CDCl_3$, ppm): δ = 7.59 (d, J = 7.6 Hz, 1H), 7.56-7.53

(m, 1H), 7.47-7.44 (m, 2H), 7.32-7.27 (m, 2H), 4.69-4.59 (m, 2H), 3.25 (s, 1H), 3.18 (s, 1H), 2.03-1.92 (m, 4H), 1.29 (d, $J = 6.1$ Hz, 6H), 1.18 (d, $J = 6.2$ Hz, 6H), 1.13-1.03 (m, 4H), 0.68 (t, $J = 7.3$ Hz, 6H), 0.64-0.53 (m, 4H).

(E)-2-Bromo-9,9-dibutyl-7-(2-(9,9-dibutyl-9H-fluoren-2-yl)vinyl)-9H-fluorene (16). In a Schlenk tube, a solution of compound **15** (3.3 g, 6.11 mmol, 1 eq) and 9,9-dibutyl-9H-fluorene-2-carbaldehyde **13** (2.1 g, 6.72 mmol, 1.1 eq) in dry THF (30 mL) was added to a solution of *t*-BuOK (2.7 g, 24.44 mmol, 4 eq) in dry THF (40 mL) at 0 °C under an argon stream. Stirring was kept at 0 °C for 1 h. The cooling bath was removed, saturated NH₄Cl (aq) was added and the mixture was extracted with ethyl acetate. The combined organic layers were dried over anhydrous Na₂SO₄, filtered and evaporated. The residue was further purified by chromatography (heptane/CH₂Cl₂ = 6/1, vol/vol), affording intermediate **16** as a white solid (3.8 g, 93%). ¹H NMR (300 MHz, CDCl₃, ppm): $\delta = 7.73$ -7.67 (m, 3H), 7.59-7.54 (m, 4H), 7.52 (s, 1H), 7.50-7.46 (m, 2H), 7.39-7.29 (m, 5H), 2.06-1.98 (m, 8H), 1.19-1.06 (m, 8H), 0.74-0.59 (m, 20H).

(E)-9,9-Dibutyl-7-(2-(9,9-dibutyl-9H-fluoren-2-yl)vinyl)-9H-fluorene-2-carbaldehyde (8). In a Schlenk tube, *n*-BuLi (1.64 mL, 2.61 mmol, 1.5 eq) was slowly added to a solution of compound **16** (1.2 g, 1.74 mmol, 1 eq) in dry THF (40 mL) at -78 °C under argon stream. Stirring was kept at -78 °C for 1 h. Then dry DMF (0.5 mL) was added and stirring was maintained at -78 °C for another 1 hour. The solution was allowed to warm up to room temperature, and the mixture was stirred for 2 h. Saturated NH₄Cl (aq) was added and the mixture was extracted with ethyl acetate. The combined organic layers were dried over anhydrous Na₂SO₄, filtered and evaporated. The residue was further purified by

chromatography (heptane/CH₂Cl₂ = 5/1, vol/vol), leading to the title compound as a yellow solid (1.0 g, 94%). ¹H NMR (300 MHz, CDCl₃, ppm): δ = 10.04 (s, 1H), 7.90-7.83 (m, 3H), 7.79 (d, *J* = 7.8 Hz, 1H), 7.73 (d, *J* = 7.8 Hz, 2H), 7.62 (dd, *J* = 8.1, 1.5 Hz, 1H), 7.59-7.56 (m, 3H), 7.40-7.30 (m, 5H), 2.15-2.01 (m, 8H), 1.19-1.06 (m, 8H), 0.73-0.54 (m, 20H). ¹³C{¹H} NMR (75 MHz, CDCl₃, ppm): δ 192.4, 152.7, 151.7, 151.2, 150.9, 147.3, 141.2, 140.7, 139.1, 138.3, 136.1, 135.2, 130.7, 129.8, 128.0, 127.1, 126.8, 125.8, 125.7, 122.9, 122.8, 121.2, 120.8, 120.7, 119.9, 119.8, 119.7, 55.2, 55.0, 40.6, 26.1, 23.2, 13.8. HRMS-ESI: *m/z* calcd for C₄₅H₅₂ONa: 631.3910; [M+Na]⁺; found: 631.3910. Anal. Calcd. (%) for C₄₅H₅₂O: C, 88.76; H, 8.61. Found: C, 87.57; H, 8.59.

2-Bromo-9,9-dibutyl-7-((E)-2-(9,9-dibutyl-7-((E)-2-(9,9-dibutyl-9H-fluoren-2-yl)vinyl)-9H-fluoren-2-yl)vinyl)-9H-fluorene (17). In a Schlenk tube, a solution of compound **15** (0.8 g, 1.52 mmol, 1eq) and aldehyde **8** (1.0 g, 1.68 mmol, 1.1 eq) in dry THF (30 mL) was added to a solution of *t*-BuOK (682 mg, 6.08 mmol, 4 eq) in dry THF (30 mL) at 0 °C under an argon stream. Stirring was kept at 0 °C for 1 h. The cooling bath was removed, saturated NH₄Cl (aq) was added and the mixture was extracted with ethyl acetate. Then the combined organic layers were dried over anhydrous Na₂SO₄, filtered and evaporated. The residue was further purified by chromatography (heptane/CH₂Cl₂ = 5/1, vol/vol), leading to intermediate **17** as a yellow solid (1.5 g, 91%). ¹H NMR (300 MHz, CDCl₃, ppm): δ 7.72-7.66 (m, 5H), 7.57-7.51 (m, 9H), 7.47-7.45 (m, 2H), 7.38-7.29 (m, 7H), 2.09-1.97 (m, 12H), 1.17-1.07 (m, 12H), 0.72-0.60 (m, 30H).

9,9-Dibutyl-7-((E)-2-(9,9-dibutyl-7-((E)-2-(9,9-dibutyl-9H-fluoren-2-yl)vinyl)-9H-fluoren-2-yl)vinyl)-9H-fluorene-2-carbaldehyde (9). In a Schlenk tube, *n*-BuLi (0.82 mL, 1.31 mmol,

2 eq) was slowly added to a solution of compound **17** (0.6 g, 0.65 mmol, 1 eq) in dry THF (30 mL) at -78 °C under an argon stream. Stirring was kept at -78 °C for 45 min, then dry DMF (0.5 mL) was added, and stirring was maintained at -78 °C for 1 h. The cooling bath was removed and the solution was allowed to warm up to room temperature. Saturated NH₄Cl (aq) was added and the mixture was extracted with ethyl acetate. The combined organic layers were dried over anhydrous Na₂SO₄, filtered and evaporated. The residue was further purified by chromatography (heptane/CH₂Cl₂ = 1/1, vol/vol), leading to the title compound as a yellow solid (425 mg, 71%). ¹H NMR (300 MHz, CDCl₃, ppm): δ = 10.07 (s, 1H), 7.89 (s, 1H), 7.86-7.82 (m, 2H), 7.79 (d, *J* = 5.9 Hz, 1H), 7.72 (d, *J* = 5.8 Hz, 4H), 7.61 (d, *J* = 6.0 Hz, 1H), 7.57-7.54 (m, 7H), 7.37-7.30 (m, 7H), 2.10-2.00 (m, 12H), 1.16-1.05 (m, 12H), 0.72-0.55 (m, 30H). ¹³C{¹H} NMR (100 MHz, CDCl₃, ppm): δ 192.3, 152.8, 151.7, 151.6, 151.3, 151.0, 147.3, 141.0, 140.9, 140.8, 140.5, 139.1, 138.4, 136.7, 136.4, 136.2, 135.2, 130.7, 129.8, 128.7, 128.5, 128.1, 127.0, 126.8, 125.9, 125.8, 125.7, 125.6, 123.0, 122.9, 121.2, 120.8, 120.7, 120.6, 120.0, 119.9, 119.9, 119.8, 119.7, 55.2, 55.0, 40.6, 40.4, 40.2, 26.0, 23.2, 23.1, 23.0, 13.9, 13.8. HRMS-ESI: *m/z* calcd for C₆₈H₇₈O: 910.60472; [M]⁺; found: 910.603. Calcd. (%) for C₆₈H₇₈O•H₂O: C, 87.88; H, 8.68. Found: C, 87.77; H, 8.52.

2-Bromo-9,9-dibutyl-7-((E)-2-(9,9-dibutyl-7-((E)-2-(9,9-dibutyl-7-((E)-2-(9,9-dibutyl-9H-fluoren-2-yl)vinyl)-9H-fluoren-2-yl)vinyl)-9H-fluoren-2-yl)vinyl)-9H-fluorene (18). In a Schlenk tube, a solution of compound **15** (281 mg, 0.52 mmol, 1 eq) and aldehyde **9** (476 mg, 0.52 mmol, 1 eq) in dry THF (15 mL) was added to a solution of *t*-BuOK (234 mg, 2.09 mmol, 4 eq) in dry THF (25 mL) at 0 °C under argon stream. Stirring was kept at 0 °C for 1 h. The cooling bath was removed, saturated NH₄Cl (aq) was added and the mixture was extracted with

ethyl acetate. Then the combined organic layers were dried over anhydrous Na₂SO₄, filtered and evaporated. The residue was further purified by chromatography (heptane/CH₂Cl₂ = 4/1, vol/vol), leading to intermediate **22** as a yellow solid (590 mg, 89%). ¹H NMR (300 MHz, CDCl₃, ppm): δ 7.73-7.65 (m, 7H), 7.61-7.50 (m, 13H), 7.48-7.44 (m, 2H), 7.37-7.28 (m, 9H), 2.09-1.97 (m, 16H), 1.17-1.07 (m, 16H), 0.73-0.60 (m, 40H).

9,9-Dibutyl-7-((E)-2-(9,9-dibutyl-7-((E)-2-(9,9-dibutyl-7-((E)-2-(9,9-dibutyl-9H-fluoren-2-yl)vinyl)-9H-fluoren-2-yl)vinyl)-9H-fluoren-2-yl)vinyl)-9H-fluorene-2-carbaldehyde (10). In a Schlenk tube, *n*-BuLi (0.35 mL, 0.55 mmol, 2 eq) was slowly added to a solution of compound **18** (350 mg, 0.28 mmol, 1 eq) in dry THF (30 mL) at -78 °C under an argon stream. Stirring was kept at -78 °C for 45 min, then dry DMF (0.2 mL) was added and stirring was maintained at -78 °C for 1 hour. The cooling bath was removed and the solution was allowed warm up to room temperature. Saturated NH₄Cl (aq) was added and the mixture was extracted with ethyl acetate. The combined organic layers were dried over anhydrous Na₂SO₄, filtered and evaporated. The residue was further purified by chromatography (heptane/CH₂Cl₂ = 4/1, vol/vol), leading to the title compound as a yellow solid (204 mg, 61%). ¹H NMR (300 MHz, CDCl₃, ppm): δ = 10.07 (s, 1H), 7.89 (s, 1H), 7.86-7.82 (m, 2H), 7.80 (d, *J* = 7.9 Hz, 1H), 7.72-7.69 (m, 6H), 7.62-7.53 (m, 12H), 7.37-7.29 (m, 9H), 2.13-1.99 (m, 16H), 1.19-1.04 (m, 16H), 0.73-0.54 (m, 40H). ¹³C {¹H} NMR (75 MHz, CDCl₃, ppm): δ = 192.3, 152.8, 151.8, 151.6, 151.3, 151.0, 147.4, 141.0, 140.9, 140.7, 140.6, 139.2, 138.4, 136.7, 136.6, 136.5, 136.2, 135.2, 130.7, 129.8, 128.7, 128.6, 128.1, 127.1, 126.8, 125.9, 125.8, 125.6, 123.0, 122.9, 121.3, 120.9, 120.8, 120.1, 120.0, 119.9, 119.7, 55.2, 55.0, 40.3, 40.2, 26.0, 23.1, 23.0, 13.9, 13.7. HRMS-ESI: *m/z* calcd for C₉₁H₁₀₄O: 1212.80817; [M]⁺; 1212.811. Anal. Calcd. (%) for C₉₁H₁₀₄O: C,

90.05; H, 8.64. Found: C, 89.81; H, 8.74.

2-Bromo-9,9-Dibutyl-7-((E)-2-(9,9-dibutyl-7-((E)-2-(9,9-dibutyl-7-((E)-2-(9,9-dibutyl-9H-fluoren-2-yl)vinyl)-9H-fluoren-2-yl)vinyl)-9H-fluoren-2-yl)vinyl)-9H-fluorene (19). In a Schlenk tube, a solution of compound **15** (93.3 mg, 0.17 mmol, 1 eq) and aldehyde **10** (210 mg, 0.17 mmol, 1 eq) in dry THF (10 mL) was added to a solution of *t*-BuOK (77.7 mg, 0.69 mmol, 4 eq) in dry THF (20 mL) at 0 °C under argon stream. Stirring was kept at 0 °C for 1 h. The cooling bath was removed, saturated NH₄Cl (aq) was added and the mixture was extracted with ethyl acetate. Then the combined organic layers were dried over anhydrous Na₂SO₄, filtered and evaporated. The residue was further purified by chromatography (heptane/CH₂Cl₂ = 4/1, vol/vol), leading to bromo intermediate **19** as a yellow solid (272 mg, 98%). ¹H NMR (400 MHz, CDCl₃, ppm): δ = 7.71-7.66 (m, 9H), 7.57-7.51 (m, 17H), 7.47-7.45 (m, 2H), 7.36-7.29 (m, 11H), 2.08-1.97 (m, 20H), 1.16-1.08 (m, 20H), 0.72-0.61 (m, 50H).

9,9-dibutyl-7-((E)-2-(9,9-dibutyl-7-((E)-2-(9,9-dibutyl-7-((E)-2-(9,9-dibutyl-7-((E)-2-(9,9-dibutyl-9H-fluoren-2-yl)vinyl)-9H-fluoren-2-yl)vinyl)-9H-fluoren-2-yl)vinyl)-9H-fluorene-2-carbaldehyde (11). In a Schlenk tube, *n*-BuLi (0.22 mL, 0.34 mmol, 2 eq) was slowly added to a solution of compound **19** (270 mg, 0.17 mmol, 1 eq) in dry THF (20 mL) at -78 °C under an argon stream. Stirring was kept at -78 °C for 45 min, then dry DMF (0.2 mL) was added and stirring was maintained at -78 °C for 1 hour. The cooling bath was removed and the solution was allowed warm up to room temperature. Saturated NH₄Cl (aq) was added and the mixture was extracted with ethyl acetate. The combined organic layers were dried over anhydrous Na₂SO₄, filtered and evaporated. The residue was further purified by

chromatography (heptane/CH₂Cl₂ = 3/1, vol/vol), leading to aldehyde **11** as a yellow solid (130 mg, 50%). ¹H NMR (400 MHz, CDCl₃, ppm): δ = 10.07 (s, 1H), 7.88-7.78 (m, 5H), 7.71-7.69 (m, 8H), 7.61-7.54 (m, 15H), 7.36-7.29 (m, 11H), 2.08-2.00 (m, 20H), 1.16-1.08 (m, 20H), 0.72-0.55 (m, 50H). ¹³C{¹H} NMR (100 MHz, CDCl₃, ppm): δ 192.3, 152.8, 151.7, 151.6, 151.3, 151.0, 147.3, 141.0, 140.9, 140.7, 140.6, 140.5, 139.1, 138.4, 136.6, 136.5, 136.2, 135.2, 130.7, 129.8, 128.7, 128.6, 128.1, 127.0, 126.8, 125.9, 125.7, 125.6, 123.0, 122.9, 121.3, 120.8, 120.6, 120.0, 119.9, 119.7, 55.2, 55.0, 40.6, 40.4, 40.2, 26.0, 23.2, 23.1, 13.9, 13.8. HRMS-MALDI: m/z calcd for C₁₁₄H₁₃₀O: 1515.0116; [M]⁺; found: 1515.0170. Anal. Calcd. (%) for C₁₁₄H₁₃₀O•heptane: C, 89.91; H, 9.10. Found: C, 88.20; H, 9.10.

Spectroscopic measurements

All photophysical properties have been performed with freshly-prepared air-equilibrated solutions at room temperature (298 K). UV-Vis absorption spectra were recorded on a BIO-TEK instrument UVIKON XL spectrometer or on a Jasco V-570 spectrophotometer in CH₂Cl_{CH} (HPLC grade). Steady-state fluorescence measurements were performed on dilute solutions (*ca.* 10⁻⁶ M, optical density < 0.1) contained in standard 1 cm quartz cuvettes using an Edinburgh Instrument (FLS920) spectrometer in photon-counting mode. Fully corrected emission spectra were obtained, for each compound, after excitation at the wavelength of the absorption maximum, with $A_{\lambda_{\text{ex}}} < 0.1$ to minimize internal absorption.^[52]

Measurements of singlet oxygen quantum yields (Φ_{Δ})

Measurements were performed on a Fluorolog-3 (Horiba Jobin Yvon), using a 450W Xenon lamp, with air-equilibrated solutions. The optical density of the reference and the sample solution were set equal to 0.15 at the excitation wavelength (maximum of the Soret band). The emission at 1272 nm was detected using a liquid nitrogen-cooled Ge-detector model (EO-817L). The emission spectra were corrected for the wavelength dependence of the lamp intensity and the excitation monochromator efficiency (excitation correction). Singlet oxygen quantum yields Φ_{Δ} were determined in CH_2Cl_2 solutions, using tetraphenylporphyrin (**4**) in CH_2Cl_2 as reference solution ($\Phi_{\Delta}[\mathbf{4}] = 0.60$) and were estimated from corrected $^1\text{O}_2$ luminescence at 1272 nm. The uncertainty of the values of the singlet oxygen quantum yields determined by this method was estimated to be ± 0.05 .

Two-Photon Absorption Experiments

To span the 790-920 nm range, a Nd:YLF-pumped Ti:sapphire oscillator (Chameleon Ultra, Coherent) was used generating 140 fs pulses at a 80 MHz rate. The excitation power is controlled using neutral density filters of varying optical density mounted in a computer-controlled filter wheel. After five-fold expansion through two achromatic doublets, the laser beam is focused by a microscope objective (10 \times , NA 0.25, Olympus, Japan) into a standard 1 cm absorption cuvette containing the sample. The applied average laser power arriving at the sample is typically between 0.5 and 40 mW, leading to a time-averaged light flux in the focal volume on the order of 0.1–10 mW/mm². The fluorescence from the sample is collected in epifluorescence mode, through the microscope objective, and reflected by a dichroic mirror

(Chroma Technology Corporation, USA; “red” filter set: 780dxcr). This makes it possible to avoid the inner filter effects related to the high dye concentrations used (10^{-4} M) by focusing the laser near the cuvette window. Residual excitation light is removed using a barrier filter (Chroma Technology; “red”: e750sp–2p). The fluorescence is coupled into a 600 μm multimode fiber by an achromatic doublet. The fiber is connected to a compact CCD-based spectrometer (BTC112-E, B&W Tek), which measures the two-photon excited emission spectrum. The emission spectra are corrected for the wavelength-dependence of the detection efficiency using correction factors established through the measurement of reference compounds having known fluorescence emission spectra. Briefly, the set-up allows for the recording of corrected fluorescence emission spectra under multiphoton excitation at variable excitation power and wavelength. 2PA cross sections (σ_2) were determined from the two-photon excited fluorescence (TPEF) cross sections ($\sigma_2 \cdot \Phi_F$) and the fluorescence emission quantum yield (Φ_F). TPEF cross-sections of 10^{-4} M CH_2Cl_2 solutions were measured relative to fluorescein in 0.01 M aqueous NaOH using the well-established method described by Xu and Webb^[53] and the appropriate solvent-related refractive index corrections.^[54] The quadratic dependence of the fluorescence intensity on the excitation power was checked for each sample and all wavelengths.

Supporting Information

Supplementary tables and figures are provided in the [Supporting Information](#): Synthesis of compound **24**, ^1H NMR and ^{13}C NMR characterization of all new compounds. The Supporting Information is available free of charge at:

Acknowledgements

The authors acknowledge CNRS for their financial support and the China Scholarship Council (CSC) for PhD funding (LS and ZS). We also thank Guillaume Clermont (ISM) for his help in the two-photon and singlet oxygen measurements.

Keywords: Porphyrinoids • Fluorene • Two-photon absorption • Oxygen sensitization • Fluorescence • Energy transfer

- [1] a) E. Buhleier, W. Wehner, F. Voegtle, *Synthesis* **1978**, 155-158; b) D. A. Tomalia, H. Baker, J. Dewald, M. Hall, G. Kallos, S. Martin, J. Roeck, J. Ryder, P. Smith, *Polym. J. (Tokyo)* **1985**, *17*, 117-132; c) G. R. Newkome, Z. Yao, G. R. Baker, V. K. Gupta, *J. Org. Chem.* **1985**, *50*, 2003-2004; d) C. J. Hawker, J. M. J. Frechet, *J. Am. Chem. Soc.* **1990**, *112*, 7638-7647; e) A. W. Bosman, H. M. Janssen, E. W. Meijer, *Chem. Rev.* **1999**, *99*, 1665-1688.
- [2] a) M. Kozaki, A. Uetomo, S. Suzuki, K. Okada, *Org. Lett.* **2008**, *10*, 4477-4480; b) A. Uetomo, M. Kozaki, S. Suzuki, K.-I. Yamanaka, O. Ito, K. Okada, *J. Am. Chem. Soc.* **2011**, *133*, 13276-13279.
- [3] a) J. N. G. Pillow, M. Halim, J. M. Lupton, P. L. Burn, I. D. W. Samuel, *Macromolecules* **1999**, *32*, 5985-5993; b) E. M. Harth, S. Hecht, B. Helms, E. E. Malmstrom, J. M. J. Fréchet, C. J. Hawker, *J. Am. Chem. Soc.* **2002**, *124*, 3926-3938; c) B. Li, K. Xu, M. Sun, Y. Fu, G. Yu, Y. Liu, Z. Bo, *Macromolecules* **2006**, *39*, 456-461; d) B. Li, J. Li, Y. Fu, Z. Bo, *J. Am. Chem. Soc.* **2004**, *126*, 3430-3431; e) M. Kozaki, K. Akita, S. Suzuki, K. Okada, *Org. Lett.* **2007**, *9*, 3315-3318.
- [4] a) P. K. Frederiksen, S. P. McIlroy, C. B. Nielsen, L. Nikolajsen, E. Skovsen, M. Jørgensen, K. V. Mikkelsen, P. R. Ogilby, *J. Am. Chem. Soc.* **2005**, *127*, 255-269; b) M. A. Oar, W. R. Dichtel, J. M. Serin, J. M. J. Frechet, J. E. Roger, J.E. Slagla, P. A. Fleiz, L. S. Tan, T. Y. Ohulchanskyy, P. N. Prasad, *Chem. Mater.* **2006**, *18*, 3682-3692.
- [5] a) C. O. Paul-Roth, J. A. G. Williams, J. Letessier, G. Simonneaux, *Tetrahedron Lett.* **2007**, *48*, 4317-4322; b) S. Drouet, C. O. Paul-Roth, *Tetrahedron* **2009**, *65*, 10693-10700; c) S. Drouet, C. O. Paul-Roth, G. Simonneaux, *Tetrahedron* **2009**, *65*, 2975-2981; d) S. Drouet, A. Merhi, G. Argouarch, F. Paul, O. Mongin, M. Blanchard-Desce, C. O. Paul-Roth, *Tetrahedron* **2012**, *68*, 98-105; e) O. Mongin, V. Hugues, M. Blanchard-Desce, A. Merhi, S. Drouet, D. Yao, C. Paul-Roth, *Chem. Phys. Lett.* **2015**, *625*, 151-156.
- [6] a) D. Yao, V. Hugues, M. Blanchard-Desce, O. Mongin, C. O. Paul-Roth, F. Paul, *New J. Chem.* **2015**, *39*, 7730-7733; b) D. Yao, X. Zhang, O. Mongin, F. Paul, C. O. Paul-Roth, *Chem. Eur. J.* **2016**, *22*, 5583-5597.

- [7] a) O. Mongin, L. Porrès, M. Charlot, C. Katan, M. Blanchard-Desce, *Chem. Eur. J.* **2007**, *13*, 1481-1498; b) G. S. He, L.-S. Tan, Q. Zheng, P. N. Prasad, *Chem. Rev.* **2008**, *108*, 1245-1330.
- [8] D. Yao, X. Zhang, S. Abid, L. Shi, M. Blanchard-Desce, O. Mongin, F. Paul, C. Paul-Roth, *New J. Chem.* **2018**, *42*, 395-401
- [9] D. Yao, X. Zhang, A. Triadon, N. Richy, O. Mongin, M. Blanchard-Desce, F. Paul, C. O. Paul-Roth, *Chem. Eur. J.* **2017**, *23*, 2635-2647.
- [10] a) R. Bonnett, *Chem. Soc. Rev.* **1995**, *24*, 19-33; b) L. B. Josefsen, R. W. Boyle, *Theranostics* **2012**, *2*, 916-966; c) J. M. Dabrowski, B. Pucelik, A. Regiel-Futyr, M. Brindell, O. Mazuryk, A. Kyzioł, G. Stochel, W. Macyk, L. G. Arnaut, *Coord. Chem. Rev.* **2016**, *325*, 67-101; d) A. Martinez De Pinillos Bayona, P. Mroz, C. Thunshelle, M. R. Hamblin, *Chem. Biol. Drug Des.* **2017**, *89*, 192-206.
- [11] a) Z. Sun, L.-P. Zhang, F. Wu, Y. Zhao, *Adv. Funct. Mater.* **2017**, *27*, 1704079; b) J. R. Starkey, A. K. Rebane, M. A. Drobizhev, F. Meng, A. Gong, A. Elliott, K. McInnerney, C. W. Spangler, *Clin. Cancer Res.* **2008**, *14*, 6564-6573; c) H. A. Collins, M. Khurana, E. H. Moriyama, A. Mariampillai, E. Dahlstedt, M. Balaz, M. K. Kuimova, M. Drobizhev, V. X. D. Yang, D. Phillips, A. Rebane, B. C. Wilson, H. L. Anderson, *Nat. Photonics* **2008**, *2*, 420-424; d) M. Khurana, H. A. Collins, A. Karotki, H. L. Anderson, D. T. Cramb, B. C. Wilson, *Photochem. Photobiol.* **2007**, *83*, 1441-1448.
- [12] a) P. Prabhu, V. Patravale, *J. Biomed. Nanotechnol.* **2012**, *8*, 859-882; b) J. Bhaumik, A. K. Mittal, A. Banerjee, Y. Chisti, U. C. Banerjee, *Nano Res.* **2015**, *8*, 1373-1394; c) H. Huang, W. Song, J. Rieffel, J. F. Lovell, *Front. Phys.* **2015**, *3*; d) J. Sandland, N. Malatesti, R. Boyle, *Photodiagnosis Photodyn. Ther.* **2018**, *23*, 281-294; e) X. Xue, A. Lindstrom, Y. Li, *Bioconjug. Chem.* **2019**, *30*, 1585-1603.
- [13] a) L. Shi, C. Nguyen, M. Daurat, A. C. Dhieb, W. Smirani, M. Blanchard-Desce, M. Gary-Bobo, O. Mongin, C. Paul-Roth, F. Paul, *Chem. Commun.* **2019**, *55*, 12231-12234; b) L. Shi, C. Nguyen, M. Daurat, N. Richy, M. Gary-Bobo, S. Cammas-Marion, O. Mongin, C. O. Paul-Roth, F. Paul, *Cancers* **2022**, *14*, 1-16.
- [14] Z. Lv, L. Zou, H. Wei, S. Liu, W. Huang, Q. Zhao, *ACS Appl. Mater. Interfaces* **2018**, *10*, 19523-19533.
- [15] Y. Wan, K. Jia, Z. Bo, A. Xia, *Sci China, Ser. B* **2009**, *52*, 56-63.
- [16] G. Grelaud, M. P. Cifuentes, F. Paul, M. G. Humphrey, *J. Organomet. Chem.* **2014**, *751*, 181-200 (150th Anniversary Special Issue).
- [17] N. C. M. Magdaong, M. Taniguchi, J. R. Diers, Dariusz M. Niedzwiedzki, C. Kirmaier, J. S. Lindsey, D. F. Bocian, D. Holten, *J. Phys. Chem. A* **2020**, *124*, 7776-7794.
- [18] J. S. Lindsey, H. C. Hsu, I. C. Schreiman, *Tetrahedron Lett.* **1986**, *27*, 4969-4970.
- [19] W. S. Wadsworth, Jr., W. D. Emmons, *Organic Syntheses* **1973**, *5*, 547-567.
- [20] X. Li, N. Markandeya, G. Jonusauskas, N. D. McClenaghan, V. Maurizot, S. A. Denisov, I. Huc, *J. Am. Chem. Soc.* **2016**, *138*, 13568-13578.
- [21] G. G. Rajeshwaran, M. Nandakumar, R. Sureshbabu, A. K. Mohanakrishnan, *Org. Lett.* **2011**, *13*, 1270-1273.
- [22] P. G. Seybold, M. Gouterman, *J. Mol. Spectroscopy* **1969**, *31*, 1-13.
- [23] L. D. Lavis, T.-Y. Chao, R. T. Raines, *ACS Chem. Bio.* **2006**, *1*, 252-260.
- [24] R. Schmidt, E. J. Afshari, *Phys. Chem. A* **1990**, *94*, 4377-4378.

- [25] O. A. Kucherak, P. Didier, Y. Mély, A. S. Klymchenko, *J. Phys. Chem. Lett.* **2010**, *1*, 616-620.
- [26] a) K. D. Belfield, M. V. Bondar, A. R. Morales, X. Yue, G. Luchita, O. V. Przhonska, O. D. Kachkovsky, *ChemPhysChem* **2012**, *13*, 3481-3491; b) O. Mongin, L. Porrès, C. Katan, T. Pons, J. Mertz, M. Blanchard-Desce, *Tetrahedron Lett.* **2003**, *44*, 9065.
- [27] D. Cao, L. Zhu, Z. Liu, W. Lin, *J. Photochem. Photobiol. C* **2020**, *44*, 100371.
- [28] T. Förster, *Faraday Soc. Discuss.* **1959**, *27*, 7-17.
- [29] A. K. Mandal, M. Taniguchi, J. R. Diers, D. M. Niedzwiedzki, C. Kirmaier, J. S. Lindsey, D. F. Bocian, D. Holten, *J. Phys. Chem. A* **2016**, *120*, 9719-9731.
- [30] H. M. Kim, B. R. Cho, *Chem. Commun.* **2009**, *45*, 153-164.
- [31] M. G. Kuzyk, *J. Mater. Chem.* **2009**, *19*, 7444-7465.
- [32] H. M. Kim, B. R. Cho, *J. Mater. Chem.* **2009**, *19*, 7402-7409.
- [33] O. Mongin, M. Sankar, M. Charlot, Y. Mir, M. Blanchard-Desce, *Tetrahedron Lett.* **2013**, *54*, 6474-6478.
- [34] S. J. Silvers, A. Tulinsky, *J. Am. Chem. Soc.* **1967**, *89*, 3331-3337.
- [35] X. Zhang, S. Abid, L. Shi, Z. Sun, O. Mongin, M. Blanchard-Desce, F. Paul, C. O. Paul-Roth, *Dyes Pigm.* **2018**, *153*, 248-255.
- [36] M. G. Kuzyk, *J. Chem. Phys.* **2003**, *119*, 8327-8334.
- [37] M. Pawlicki, H. A. Collins, R. G. Denning, H. L. Anderson, *Angew. Chem. Int. Ed.* **2009**, *48*, 3244-3266.
- [38] F. Paul, C. Lapinte, *Coord. Chem. Rev.* **1998**, *178/180*, 431-509.
- [39] J. Zhao, D. Zhong, S. Zhou, *Mater. Chem. B* **2018**, *6*, 349-365.
- [40] D. Yao, L. Shi, Z. Sun, M. Blanchard-Desce, O. Mongin, F. Paul, C. O. Paul-Roth, *C. R. Chim.* **2021**, *24*, 57-70.
- [41] M. Drobizhev, Y. Stepanenko, Y. Dzenis, A. Karotki, A. Rebane, P. N. Taylor, H. L. Anderson, *J. Phys. Chem. B* **2005**, *109*, 7223-7236.
- [42] F. Bolze, S. Jenni, A. Sour, V. Heitz, *Chem. Commun.* **2017**, *53*, 12857-12877.
- [43] T. C. Pham, V.-N. Nguyen, Y. Choi, S. Lee, J. Yoon, *Chem. Rev.* **2021**, *121*, 13454-13619.
- [44] J.-X. Zhang, J.-W. Zhou, C.-F. Chan, T. C.-K. Lau, D. W. J. Kwong, H.-L. Tam, N.-K. Mak, K.-L. Wong, W.-K. Wong, *Bioconjugate Chem.* **2012**, *23*, 1623-1638.
- [45] Note however that ill-defined (polymeric) species resembling A^n were tested in 2PA-PDT.^[15]
- [46] a) M. Drobizhev, Y. Stepanenko, Y. Dzenis, A. Karotki, A. Rebane, P. N. Taylor, H. L. Anderson, *J. Am. Chem. Soc.* **2004**, *126*, 15352-15353; b) A. Karotki, M. Drobizhev, Y. Dzenis, P. N. Taylor, H. L. Anderson, A. Rebane, *Phys. Chem. Chem. Phys.* **2004**, *6*, 7-10.
- [47] F. Hammerer, S. Achelle, P. Baldeck, P. Maillard, M.-P. Teulade-Fichou, *J. Phys. Chem. A* **2011**, *115*, 6503-6508.
- [48] J. Schmitt, V. Heitz, A. Sour, F. Bolze, H. Ftouni, J.-F. Nicoud, L. Flamigni, B. Ventura, *Angew. Chem. Int. Ed.* **2015**, *54*, 169-173.
- [49] F. Ding, Y. Zhan, X. Lu, Y. Sun, *Chem. Sci.* **2018**, *9*, 4370-4380.
- [50] M. M. Alam, F. Bolze, C. Daniel, L. Flamigni, C. Gourlaouen, V. Heitz, S. Jenni, J. Schmitt, A. Sourd, B. Ventura, *Phys. Chem. Chem. Phys.* **2016**, *18*, 21954-21965.

- [51] D. D. Perrin, W. L. F. Armarego, *Purification of Laboratory Chemicals*, 3rd ed., Pergamon Press, Oxford, **1988**.
- [52] a) N. Demas, G. A. Crosby, *J. Phys. Chem.* **1971** 75, 991-1024; b) G. R. Eaton, S. S. Eaton, *Acc. Chem. Res.* **1988**, 21, 107-113.
- [53] C. Xu, W. W. Webb, *J. Opt. Soc. Am. B* **1996**, 13, 481-491.
- [54] M. H. V. Werts, N. Nerambourg, D. Pélégry, Y. Le Grand, M. Blanchard-Desce, *Photochem. Photobiol. Sci.* **2005**, 4, 531-538.

- Table of Contents (ToC) entry (a.k.a. graphical abstract):

New Starburst porphyrins possessing up to twenty conjugated fluorenyl units have been synthesized. Their detailed oxygen-photosensitizing ability, their fluorescence and their two-photon absorption properties are discussed

